HHS Public Access

Author manuscript

Cell Rep. Author manuscript; available in PMC 2022 August 17.

Published in final edited form as:

Cell Rep. 2021 August 17; 36(7): 109522. doi:10.1016/j.celrep.2021.109522.

The angiopoietin-Tie2 pathway regulates Purkinje cell dendritic morphogenesis in a cell-autonomous manner

Robert Luck[1], **Andromachi Karakatsani**[1], **Bhavin Shah**[1], **Geza Schermann**[1], **Heike Adler**[1], **Janina Kupke**[2], **Nathalie Tisch**[1], **Hyun-Woo Jeong**[3], **Michaela Kerstin Back**[4], **Florian Hetsch**[4], **Anna D'Errico**[8], **Michele De Palma**[5], **Ellen Wiedtke**[6], **Dirk Grimm**[6,7], **Amparo Acker-Palmer**[8], **Jakob von Engelhardt**[4], **Ralf H. Adams**[3], **Hellmut G. Augustin**[1,9], **Carmen Ruiz de Almodóvar**[1,10,*]

[1]European Center of Angioscience (ECAS), Medical Faculty Mannheim, University of Heidelberg, 68167 Mannheim, Germany

[2]Department of Neurobiology, Interdisciplinary Centre for Neurosciences (IZN), University of Heidelberg, 69120 Heidelberg, Germany

[3]Department of Tissue Morphogenesis, Max Planck Institute for Molecular Biomedicine, and University of Münster, Faculty of Medicine, 48149 Münster, Germany

[4]Institute of Pathophysiology, Focus Program Translational Neuroscience (FTN), University Medical Center of the Johannes Gutenberg University Mainz, 55131 Mainz, Germany

[5]Swiss Institute for Experimental Cancer Research (ISREC), Swiss Federal Institute of Technology in Lausanne (EPFL), 1015 Lausanne, Switzerland

[6]Department of Infectious Diseases/Virology, Medical Faculty, University of Heidelberg, Bioquant Center, 69120 Heidelberg, Germany

[7]German Center for Infection Research (DZIF), and German Center for Cardiovascular Research (DZHK), Heidelberg, Germany

[8]Institute of Cell Biology and Neuroscience and Buchmann Institute for Molecular Life Sciences (BMLS), University of Frankfurt, 60323 Frankfurt, Germany

[9]Division of Vascular Oncology and Metastasis, German Cancer Research Center Heidelberg (DKFZ-ZMBH Alliance), 69120 Heidelberg, Germany

*Correspondence: carmen.ruizdealmodovar@medma.uni-heidelberg.de.

AUTHOR CONTRIBUTIONS

Conceptualization, R.L. and C.R.d.A.; methodology, R.L., M.K.M., F.H., A.D., and E.W.; software, G.S.; formal analysis, R.L., A.K., B.S., G.S., J.K., N.T., M.K.M., F.H., and A.D.; investigation, R.L., A.K., B.S., G.S., H.A., J.K., N.T., M.K.M., F.H., A.D., and E.W.; resources, M.D.P., D.G., A.A.P., J.v.E., H.G.A., and C.R.d.A.; writing – original draft, R.L. and C.R.d.A.; writing – review & editing, R.L., A.K., B.S., G.S., N.T., A.D., D.G., A.A.P., J.v.E., R.H.A., H.G.A., and C.R.d.A.; visualization, R.L. and C.R.d.A.; supervision, C.R.d.A.; funding acquisition, A.A.P., R.H.A., H.G.A., and C.R.d.A.

SUPPLEMENTAL INFORMATION

Supplemental information can be found online at https://doi.org/10.1016/j.celrep.2021.109522.

DECLARATION OF INTERESTS

The authors declare no competing interests.

INCLUSION AND DIVERSITY

One or more of the authors of this paper self-identifies as a member of the LGBTQ+ community.

[10]Lead contact

SUMMARY

Neuro-vascular communication is essential to synchronize central nervous system development. Here, we identify angiopoietin/Tie2 as a neuro-vascular signaling axis involved in regulating dendritic morphogenesis of Purkinje cells (PCs). We show that in the developing cerebellum Tie2 expression is not restricted to blood vessels, but it is also present in PCs. Its ligands angiopoietin-1 (Ang1) and angiopoietin-2 (Ang2) are expressed in neural cells and endothelial cells (ECs), respectively. PC-specific deletion of Tie2 results in reduced dendritic arborization, which is recapitulated in neural-specific Ang1-knockout and Ang2 full-knockout mice. Mechanistically, RNA sequencing reveals that Tie2-deficient PCs present alterations in gene expression of multiple genes involved in cytoskeleton organization, dendritic formation, growth, and branching. Functionally, mice with deletion of Tie2 in PCs present alterations in PC network functionality. Altogether, our data propose Ang/Tie2 signaling as a mediator of intercellular communication between neural cells, ECs, and PCs, required for proper PC dendritic morphogenesis and function.

In brief

Luck et al. describe a mechanism regulating Purkinje cell dendritic morphogenesis. They show that Tie2 signaling acts in a cell-autonomous manner in Purkinje cells. The ligands, Ang1 and Ang2, are expressed in neural and endothelial cells, respectively. This pathway is required for proper dendritic morphogenesis and neuronal functionality.

Graphical Abstract

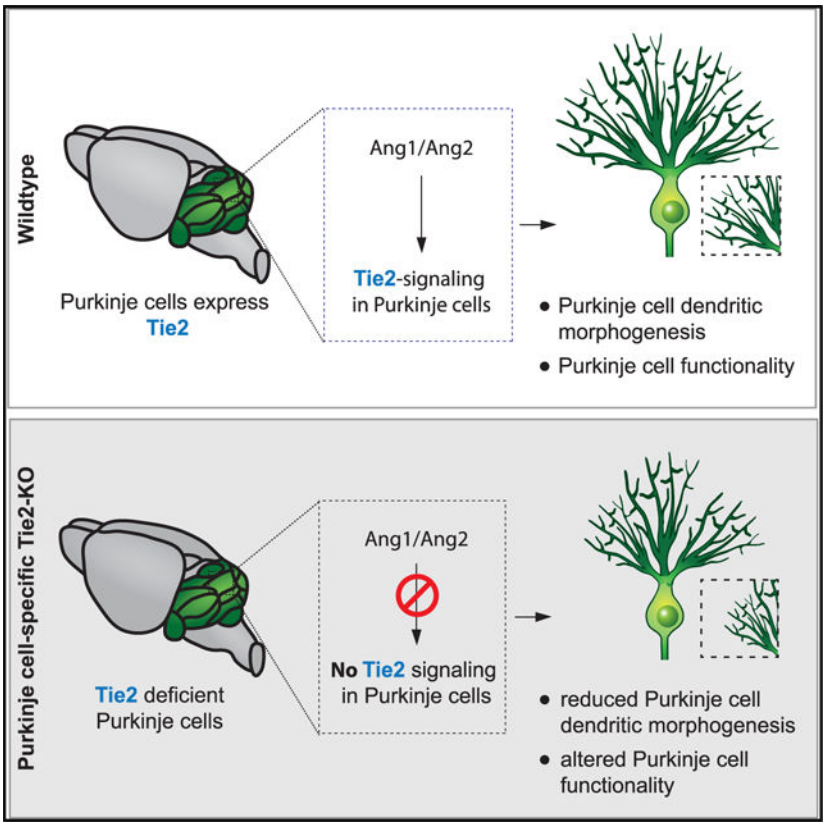

INTRODUCTION

Research of the last decade has shown that factors involved in the development of the nervous system are also required to regulate blood vessel growth and guidance, and vice versa. Furthermore, the intercellular communication between vascular and neural cells (neural progenitors, neurons, and glia) is crucial for the proper development and function of the central and peripheral nervous systems (Paredes et al., 2018; Segarra et al., 2019). However, the molecular determinants that both systems use to communicate are poorly understood. While most studies in this context have focused on characterizing particular aspects of this neurovascular crosstalk in the developing cortex, spinal cord, and retina (Paredes et al., 2018), the cerebellum, and how neurovascular mechanisms might regulate dendritic morphogenesis, has been largely unexplored.

Cerebellar function has been linked to sensory-motor processing (D'Angelo et al., 2011), as well as to the coordination of emotions (e.g., reward seeking and anxiety) and diverse aspects of cognition (e.g., spatial learning and navigation) (Adamaszek et al., 2017; Koziol et al., 2014; Wang and Zoghbi, 2001). In mice, the formation of the cerebellum starts during embryonic stages and continues postnatally (Butts et al., 2014). The mature cerebellum contains several types of excitatory and inhibitory neurons, organized in a three-layered structure: from outside to inside—the molecular layer (ML), the Purkinje cell layer (PCL), and the internal granular layer (IGL) (Butts et al., 2014). PCs represent the main GABAergic cell type, integrating motor, and sensory information derived from an array of parallel fibers

and a single climbing fiber input. The PC soma is positioned in the PCL (a single cell layer), and its extensively branched dendritic tree expands into the ML. PC dendrites project in a planar fashion, oriented in parallel to the anterior-posterior axis of the brain (Leto et al., 2016). PC dendritic morphogenesis starts postnatally and proceed during a long period of time up to at least 3 months of age (McKay and Turner, 2005). It is regulated by cellular mechanisms involving dendritic growth, branching, dendritic self-avoidance, retraction processes, and maturation, which assures precise integration of inputs and propagation of signals (Takeo et al., 2015). Several signaling molecules have been described to regulate PC morphogenesis, among them Slit/Robo signaling (Gibson et al., 2014), Protocadherins (Ing-Esteves et al., 2018; Lefebvre et al., 2012; Toyoda et al., 2014), tropomyosin receptor kinase C (TrkC) (Huang et al., 2014; Joo et al., 2014), and thyroid hormone receptor a1 (TRa1) (Heuer and Mason, 2003), among others. Remarkably, at the same time as PCs are extending and positioning their dendritic trees, blood vessels are growing and branching in close vicinity. This also occurs within an environment of glia cells (Buffo and Rossi, 2013). If and how growing blood vessels, glia cells, and neurons communicate during cerebellum formation to assure proper PC dendritic morphogenesis remains unknown.

The angiopoietin-Tie signaling pathway is crucial for blood vessel formation, assembly, maturation, and homeostasis (Augustin et al., 2009). In ECs, Tie2 is the main protein tyrosine kinase receptor that is activated by angiopoietin ligands. Its activation is tightly regulated by the ratio of Ang1/Ang2 expression. While Ang1-induced signaling mediates EC survival and maturation, Ang2 can either counteract Ang1 or induce Tie2 activation in a context-dependent manner (Augustin et al., 2009). Tie2 activation is further regulated by the presence or absence of its co-receptor Tie1 (Hansen et al., 2010; Savant et al., 2015). Concerning CNS development, several studies (mainly *in vitro*) suggest a potential role of the angiopoietins in regulating neuronal progenitor proliferation, differentiation, migration, survival, and branching (Bai et al., 2009; Kosacka et al., 2005; Marteau et al., 2011; Rosa et al., 2010; Ward et al., 2005). However, the *in vivo* characterization of their effects on neurons is still missing. In addition, *in vivo* proof of whether the receptor Tie2 is expressed in certain neuronal types, and if the observed effects occur via direct signaling to Tie2 in neurons is lacking.

In this study, we describe a cell-autonomous role for Tie2 in PCs as a modifier of dendritic morphogenesis. Using *in vivo* mouse genetics for Ang1, Ang2, and Tie2, we identify the AngTie2 pathway as a neural-vascular-PC intercellular communication axis that regulates PC dendritic morphogenesis, with Tie2 acting in a PC cell-autonomous fashion. Unbiased analysis of the PC translatome indicates that the absence of Tie2 in PCs leads to deregulated expression of proteins involved in cytoskeleton dynamics and neurite branching. At the functional level, we show that Tie2-deficient PCs present altered network electrophysiological properties.

RESULTS

Ang1, Ang2, and Tie2 are expressed in different cell types during postnatal cerebellar development

We analyzed the temporal expression of angiopoietin ligands and their Tie2 receptor in the entire developing cerebellum. In the first postnatal week, *Ang1* mRNA expression levels increased and peaked at P7. Subsequently, mRNA levels gradually diminished (Figure S1A). Consistently, *in situ* hybridization (ISH) showed that *Ang1* mRNA was detected in the white matter (WM) of the cerebellum as well as in the IGL (Figure 1A). Ang1 mRNA expression declined in later stages (Figures S1A and S1B). To determine the cellular source of Ang1 we analyzed an available single cell RNA sequencing (scRNA-seq) dataset of the developing murine cerebellum (Carter et al., 2018). In this dataset, Ang1 expression was found in the majority of GABAergic interneurons, in pial vessels and in a subpopulation of astrocytes (Figure S1C). To verify these results, we performed ISH combined with immunofluorescent (IF) staining on postnatal cerebellar tissue at different developmental stages (from P3 to P21). Consistent with the analysis of Ang1 expression using the scRNA-seq dataset, *Ang1* mRNA colocalized with the GABAergic interneuron lineage marker Pax2 (Fleming et al., 2013; Maricich and Herrup, 1999; Figure 1B). Ang1 expression also colocalized with GFAP-expressing astrocytes located in the WM and the IGL (Figure 1C), which is consistent with previously published data (Baldwin et al., 2001).

The temporal course of *Ang2* mRNA expression in the whole cerebellum was less dynamic (Figure S1D). Expression of *Ang2* mRNA was found in ECs at all developmental stages analyzed, as previously described (Fiedler et al., 2006; Figure 1D).

Next, we analyzed the expression of the angiopoietin receptor Tie2 using a previously described Tie2-GFP reporter mouse line (De Palma et al., 2005). GFP expression was not just restricted to blood vessels of the postnatal cerebellum but was also observed in cerebellar PCs at P7 and P9 (Figure 1E; Figure S1E) and adult (Figure S1E). Of note, GFP signal was also detected in pyramidal neurons of the developing hippocampus (Figure S1F). Expression of *Ang1* mRNA was also observed in the developing hippocampus (Figure S1G). To confirm the expression of Tie2 in PCs, we made use of the RiboTag mouse line, in which a modified ribosomal protein Rpl22 is tagged with an HA epitope and expressed in a Cre-dependent manner (Sanz et al., 2009). We crossed a PC-specific Cre driver line (Pcp2Cre; Barski et al., 2000) with RiboTag mice to assure specific expression in PCs (from here on Pcp2Cre:Rpl22$^{HA/HA}$). The temporal expression of Cre recombinase in the driver line and its functionality was assessed by ISH of *Cre* mRNA as well as by using the ROSA-mTmG reporter line (from here on Pcp2Cre:mTmG) at different postnatal stages (Muzumdar et al., 2007). These approaches showed that Cre expression and activity started around P7 in a small number of PCs and that the majority of PCs expressed functional Cre recombinase by P21 (Figures S1H and S1I). Considering the temporal expression of Cre recombinase in PCs, we immunoprecipitated the HA-Rpl22 subunit together with its associated mRNA from cerebellar lysates of Pcp2Cre:Rpl22$^{HA/HA}$ animals at different time points starting from P10 and analyzed expression of Tie2 in the associated mRNA. *Tie2* mRNA was detectable after ribosomal pull-down in all tested stages (Figure S1J). Finally, to verify that *Tie2* mRNA

was expressed in PCs, we crossed Pcp2Cre:Rpl22$^{HA/HA}$ mice with Tie2$^{flox/flox}$ animals (Savant et al., 2015) to generate triple-transgenic Pcp2Cre:Tie2$^{flox/flox}$:Rpl22$^{HA/HA}$ mice, in which a reduction of *Tie2* mRNA should be detected after HA-Rpl22 pull-down, when compared to Pcp2Cre:Rpl22$^{HA/HA}$ animals. Indeed, *Tie2* mRNA expression was reduced in the triple-transgenic mice as early as P10 (Figure S1M), confirming the expression of Tie2 in PCs.

Taken together, the time points when Tie2 and its ligands Ang1 and Ang2 were expressed in the developing cerebellum coincided with the critical period of PC dendritic morphogenesis. This suggests that the angiopoietin-Tie2 signaling axis could be an intercellular communication mechanism via which neural cells, ECs, and PCs crosstalk to regulate PC development. As Tie2 is expressed in PCs during this developmental period, this also suggests that Tie2 might exert a cell-autonomous function in PCs.

Tie2 expression in postnatal PCs regulates dendritic development and maintenance

The expression of Tie2 in PCs led us to investigate whether Tie2 regulated the dendritic development of these neurons *in vivo*, in a cell-autonomous manner. For this, we analyzed PC dendritic morphogenesis in Pcp2Cre$^{+/-}$:Tie2$^{flox/flox}$ mice (in which Tie2 was specifically deleted in PCs; termed from hereon Pcp2Cre:Tie2$^{flox/flox}$) and control littermates (Pcp2Cre$^{-/-}$:Tie2$^{flox/flox}$; termed from hereon Tie2$^{flox/flox}$). Pcp2Cre:Tie2$^{flox/flox}$ animals showed no obvious differences in cerebellar anatomy, density of PC soma, or bodyweight when compared to control mice (Figures 2A–2D). PC dendritic branching was analyzed by stereotactic injection of low concentrations of AAV serotype 8 encoding YFP (AAV8-YFP, which has a tropism for PCs; Gibson et al., 2014) into the cerebellum of P7, P42, or 6-month-old mice, allowing us to reconstruct PC dendritic arbors at the single-cell level upon imaging (Figures S2A–S2C). Mice were sacrificed 2 weeks post-injection, and the number of PC dendritic branches as well as the total dendritic length were analyzed (see STAR Methods and Figure S2 for further details of the analysis). This revealed that Pcp2Cre:-Tie2$^{flox/flox}$ mice lost dendritic complexity over time. While initially the number of branches was slightly increased at P21 (Figures 2E–2G), PC dendritic complexity at later stages was characterized by a reduced number of both dendritic branches and total dendritic length (Figures 2H–2M). Notably, we also observed changes in the ordered array of the dendritic field (Figures 2E, 2H, and 2K). Interestingly, similar defects in dendritic morphogenesis were observed in heterozygous Pcp2Cre:Tie2$^{+/flox}$ animals (Figures S3A–S3C and S3G–S3I). Pcp2Cre$^{+/-}$ mice (from here on Pcp2Cre; Pcp2Cre$^{-/-}$ animals from here on referred to as WT) were analyzed as an additional control. These mice did not show any differences in cerebellar anatomy, the density of PC soma and bodyweight, or in PC dendritic morphology (Figures S4A–S4G), indicating that it is the absence of Tie2 in PCs that leads to the observed dendritic branching phenotype and not the expression of Cre recombinase.

In summary, our analysis revealed that Tie2 in PCs contributes to the regulation of dendritic morphogenesis in a cell-autonomous manner. The fact that Pcp2Cre:Tie2$^{flox/flox}$ mice showed a slight increase in PC branching at P21, which is not maintained at later

developmental stages, suggests that a compensatory mechanism might be active in early development, but this is not sufficient to compensate for the absence of Tie2.

Nervous-system-specific deletion of Ang1 and constitutive Ang2 knockout lead to reduced PC dendritic complexity

Next, we asked whether changes in the expression of the Tie2 ligands Ang1 and Ang2 would also impair PC dendritic morphogenesis. To investigate the role of Ang1 in the developing cerebellum, we crossed $Ang1^{flox/flox}$ mice (provided by Susan E. Quaggin [Jeansson et al., 2011]) with the Nestin-Cre driver line (Tronche et al., 1999). Nestin-Cre recombines in all cells derived from Nestin-expressing neural progenitors (Wojcinski et al., 2017), including interneurons and astrocytes, where we detected Ang1 expression during cerebella development. Ang1 deletion was confirmed by ISH (Figure S5A) and qPCR (Figures S5B and S5D). Genetic inactivation of Ang1 expression did not affect *Ang2* mRNA levels (Figures S5C and S5E). The overall anatomy of the cerebellum and the density of PC soma were unchanged in NesCre:$Ang1^{+/flox}$ and NesCre:$Ang1^{flox/flox}$ animals (Figures 3A– 3C), despite the fact that both genotypes showed a reduction in bodyweight at P21 compared to their Cre-negative littermates (Figure 3D).

Using the same AAV8 approach, we then studied PC dendritic development in NesCre:$Ang1^{+/flox}$ and NesCre:$Ang1^{flox/flox}$ animals. PCs showed lower dendritic complexity already at P21, with a reduced number of dendritic branches in both genotypes, and reduced total dendritic length in NesCre:$Ang1^{flox/flox}$ animals, when compared to control littermates (Figures S5F–S5H). This phenotype was even more severe at P56 (Figures 3E–3G). Similarly, dendritic length of *in vivo* CA1 hippocampal neurons of NesCre:$Ang1^{flox/flox}$ pups (measured from Golgi staining) was also reduced compared to control mice (Figures S5I and S5J). These data suggested that Ang1-Tie2 signaling in Tie2-expressing neurons might be required to promote the development of dendritic branches. To test this hypothesis in PCs, we used an *in vitro* approach using cerebellar slice cultures. Cerebellar slices from P6 mice were cultured with or without recombinant Ang1 for 3 days *in vitro* (DIV). Analysis of PC dendrites showed that Ang1 stimulation resulted in a significant increase in both the number of branches and branch length (Figures 3H–3J). Taken together, these data show that Ang1 promoted dendritic growth and branching in CNS neurons. *In vivo*, neural loss of Ang1 led to a reduction in PC dendritic complexity, which recapitulated the phenotype observed in PC-specific Tie2 knockout mice. Based on the expression pattern of Ang1, our data suggest that direct binding of neural-derived Ang1 to Tie2 in PCs might induce a signaling cascade to regulate dendritic development.

We next studied whether Ang2 would also contribute to PC dendritic development using homo- and heterozygous Ang2 full knockout mice (from hereon $Ang2^{+/-}$ and $Ang^{-/-}$) (Gale et al., 2002). Reduction of cerebellar *Ang2* mRNA was confirmed in whole-tissue lysates of P21 mice (Figure S5K). Levels of *Ang1* mRNA were unchanged in $Ang2^{+/-}$ and $Ang2^{-/-}$ animals (Figure S5L). The overall anatomy of the cerebellum, including the thickness of the ML as well as the density of PC somas, was unchanged (Figures 3K–3M). However, $Ang2^{-/-}$ mice had significantly reduced bodyweight at P21 compared to their WT littermates (Figure 3N). At P21, a significant reduction in the number of dendritic

branches as well as the total dendritic length was observed in Ang2$^{-/-}$ animals but not in Ang2$^{+/-}$ mice (Figures S5M–S5O). At P56, both Ang2$^{+/-}$ and Ang2$^{-/-}$ animals showed a strong reduction of dendritic arborization (Figures 3O–3Q). Thus, Ang2 deficiency also resulted in reduced dendritic complexity of PCs. Altogether, the data suggested that the angiopoietin-Tie2 signaling axis contributed to the development and long-term maintenance of PC dendrites.

In PCs, dendritic self-avoidance (repulsion between branches of the same neuron) and acquisition of dendritic planarity are crucial steps to achieve proper morphology and functionality (Ing-Esteves et al., 2018; Lefebvre et al., 2012; Toyoda et al., 2014). This process can occur independently of dendritic branching (Gibson et al., 2014). We questioned whether, besides dendritic branching, the Ang-Tie2 signaling axis would also regulate dendritic self-avoidance and planarity. NesCre:Ang1$^{flox/flox}$ mice showed an increase in dendritic crosses at P21 that strongly inverted at P56 (Figures S6A and S6D). Concomitantly, PCs lost their dendritic planarity over time as indicated by an increased spread of branch endpoints as well as an increased planar width in the Z axis (Figures S6B, S6C, S6E, and S6F). In contrast to the NesCre:Ang1$^{flox/flox}$ animals, Ang2$^{-/-}$ mice showed a significant reduction in the number of dendritic crosses at P21, which normalized between genotypes in later stages (Figures S6G and S6J). Dendritic planarity was not affected in Ang2$^{-/-}$ mice (Figures S6H, S6I, S6K, and S6L). No differences were observed in Pcp2Cre:Tie2$^{flox/flox}$ and Pcp2Cre:-Tie2$^{+/flox}$ (Figures S6M–S6U and Figures S3D–S3F and S3J–S3L). Altogether, the data suggest either that Tie2 in PCs is only required to regulate dendritic branching but not self-avoidance or that a compensatory mechanism prevents a self-avoidance phenotype in the absence of Tie2 receptor (see also Discussion).

Cerebellar vasculature is mildly affected in NesCre:Ang1$^{flox/flox}$ and Ang2$^{-/-}$ mice

Our data so far indicate a cell-autonomous function of the angiopoietin-Tie2 signaling axis when studying Pcp2Cre:Tie2$^{flox/flox}$ mice. To further investigate whether changes in the vasculature could indirectly contribute to the observed PC branching phenotype, we analyzed the Ang1 and Ang2 transgenic mice. More specifically, we analyzed blood vessel development in the cerebellum of NesCre:Ang1$^{+/flox}$ and NesCre:Ang1$^{flox/flox}$, as well as Ang2$^{+/-}$ and Ang2$^{-/-}$ animals. While heterozygous mice for both ligands (NesCre:Ang1$^{+/flox}$ and Ang2$^{+/-}$) did not show any vascular defects, homozygous mice had a mild morphological phenotype (Figures 4A–4H). Consistent with Angiopoietin ligands function in the vascular system, NesCre:Ang1$^{flox/flox}$ animals presented a mild increase in blood vessel length at P21 and P56 in the outer layers of the cerebellum (Figures 4A–4D), whereas Ang2$^{-/-}$ mice showed a mild reduction in blood vessel length in the cerebellum (Figures 4E–4H). Pericyte coverage was not affected in the transgenic mouse lines at the different time points analyzed (Figures 4I–4L).

Taken together, neural loss of Ang1 and Ang2-deficiency mildly affected the patterning of cerebellar vascularization. The fact that (1) heterozygous mice showed PC dendritic branching defects but no vascular phenotype and (2) the PC-specific deletion of Tie2 also resulted in a PC dendritic arborization phenotype supports our hypothesis that angiopoietin-Tie2 signaling controlled PC dendritic branching in a cell-autonomous manner. However,

the experiments could not completely rule out the possibility that the aberrant blood vessel patterning in homozygous knockout animals also contributed to the observed PC dendritic arborization defects.

Tie2-deficient PCs present alterations in the expression of genes involved in neuronal wiring

We next aimed to investigate in further detail the molecular mechanisms behind the observed PC dendritic arborization phenotype. For this, we used the triple transgenic mouse line Pcp2Cre: Tie2$^{flox/flox}$:Rpl22$^{HA/HA}$ to isolate and sequence mRNAs being translated specifically in PCs lacking Tie2 at P56. As control, we also isolated and sequenced mRNAs being translated in PCs from P56 Pcp2Cre:Rpl22$^{HA/HA}$ mice. Analysis of the sequencing data showed a total number of 4,147 differentially expressed genes, among them having 1,889 genes upregulated and 2,258 genes downregulated (Table S1; Figure 5A). These differentially expressed genes were characterized using ingenuity pathway analysis (IPA), which provides a list of affected pathways from all aspects of cell biology (Krämer et al., 2014). Consistent with a defect in dendritic morphogenesis, the output from IPA remarkably indicated that functions such as cytoskeleton organization, development of neurons, neuritogenesis, outgrowth of neurons, and neurites as well as formation of dendrites were significantly changed in Tie2-deficient PCs (Figures 5B–5F; Figures S7A–S7G; Table S2). Genes within those functional categories included multiple receptors, ligands, and intracellular signaling molecules known to regulate neurite outgrowth and branching (e.g., Bdnf, Cxcl12, Netrin1, Sema3B, Ntrk3/TrkC, EphB8, EphB1, Dscam, Ryk). In addition, the expression of molecules regulating cytoskeleton dynamics (e.g., Cdc42, Rap1Gap, Wasf1), the cytoskeleton structural component Tubb3 (Tubulin beta 3 Class III), and microtubule dynamics were also altered (Figures 5C and 5D; Figures S7F and S7G). Altogether, the sequencing data indicate that absence of Tie2 specifically in PCs results in expression changes of a pool of genes involved in neuronal development, dendritogenesis, and dendritic branching. These data also suggest that Tie2 activation in PCs leads to the regulation of multiple genes, which most likely participate in different steps of dendritic morphogenesis (growth, branching, etc.) and together shape the dendritic tree of these neurons.

Loss of Tie2 expression in postnatal PCs results in alterations of cerebellum network functionality

Next, we questioned whether the morphological differences seen in Pcp2Cre:Tie2$^{flox/flox}$ are accompanied by changes on the level of synapses and neuronal electrophysiological properties of PCs. Analysis of dendritic spines in AAV8-infected PCs of the Pcp2Cre:Tie2$^{flox/flox}$ line revealed an increased density of distal spines in all stages analyzed (P21, P56, and 6 months) compared to control mice (Figures 6A–6D). No difference was detected in Pcp2Cre$^{+/-}$ versus Pcp2Cre$^{-/-}$ mice (Figures S4K and S4L). Next, PCs from 8- to 11-week-old Pcp2Cre;Tie2$^{flox/flox}$ mice were patched and recorded to analyze inputs from parallel fibers (mEPSCs) and from GABAergic interneurons (mIPSCs) as described before (Zhang et al., 2015). Consistent with the increase in spine number, PCs from 8–11-week-old Pcp2Cre;Tie2$^{flox/flox}$ animals showed increased mEPSC frequency, albeit its amplitude was unchanged (Figures 6E–6H). mIPSC characteristics were not affected upon

deletion of Tie2 (Figures 6I–6L). Last, an additional set of PCs from 8- to 11-week-old Pcp2Cre;Tie2$^{flox/flox}$ animals was patched to analyze their spontaneous activity (spontaneous tonic firing). These electrophysiological recordings showed that spontaneous tonic firing was reduced in Pcp2Cre;Tie2$^{flox/flox}$ animals compared to controls (Figures 6M–6P).

Collectively, these data suggest that PC function and network is altered in animals lacking Tie2 in PCs.

DISCUSSION

In this study, we identified a previously undescribed nonvascular role of Tie2 in PCs. We document a role for the angiopoietin-Tie2 pathway as an intercellular communication axis between distinct cell types in the cerebellum during development. We describe a cell-autonomous role for Tie2 in PCs that contributes to the regulation of dendritic morphogenesis, and we also show that angiopoietin ligands derived from the neural and endothelial compartments are important for this process (Figure 7).

The expression profiling experiments in this study demonstrate that the cognate angiopoietin receptor Tie2, apart from being expressed in the vasculature, is also expressed in PCs of the cerebellum. So far, expression of Tie2 has mainly been described in ECs (Augustin et al., 2009), pericytes, and a subpopulation of monocytes termed TEMs (Tie2-expressing monocytes) (Teichert et al., 2017; Venneri et al., 2007). In the context of neural cells, Tie2-expression has only been reported in neuronal progenitor cells (NPCs) (Androutsellis-Theotokis et al., 2009; Liu et al., 2009; Parati et al., 2002; Rosa et al., 2010). Our study adds to this knowledge and reports expression of Tie2 in differentiated neurons of the cerebellum (PCs) and the hippocampus (pyramidal neurons). Consistent with a previous study (Baldwin et al., 2001), we show that angiopoietins are expressed in the postnatal developing cerebellum during a temporal window when high PC dendritic morphogenesis and cerebellar vascularization take place. These observations are in line with previous reports that describe astrocytes and ECs as the cellular source of Ang1 and Ang2, respectively (Fiedler et al., 2006; Michinaga et al., 2020; Ward et al., 2005). Here, we extend those findings and further show that Ang1 is also expressed in GABAergic interneurons. These combined expression patterns, together with our functional *in vivo* analysis (see below for further discussion), suggest that a controlled inter-neural-vascular communication is required for proper cerebellar development.

The role of the Ang-Tie2 signaling axis in neurodevelopment processes *in vivo* was so far little characterized. In our study, we show that Tie2 expression in cerebellar PCs has a cell-autonomous role in regulating PC dendritic morphogenesis. The observed morphological changes of dendritic branching are in a similar range as those occurring reported before (Gibson et al., 2014; Kawabata Galbraith et al., 2018; Kuwako and Okano, 2018). PC-specific loss of Tie2 resulted in a transient increase in dendritic branching at earlier time points, which, however, was not maintained and finally led to a reduced dendritic complexity at later stages. This transient increase might be interpreted as compensatory reaction of PCs trying to compensate for the lack of Tie2. This compensatory mechanism, although active at early time points, is not sufficient, and PCs end up with reduced dendritic branches.

Moreover, our data might also suggest that Tie2 receptor in PCs is required for dendritic maintenance. A similar role is attributed to Tie2 in the vascular context, where Tie2 expression is essential during embryogenesis but also contributes to the maintenance of vessels in postnatal stages (Augustin et al., 2009).

A variety of extracellular signaling molecules, membrane receptors, and intracellular signaling components have been described to regulate dendritic morphogenesis. These include Slits, BDNF, Ryk, TrkC, PKCγ, NF-κB-RelA, and mTOR signaling molecules among others (Angliker et al., 2015; Fujishima et al., 2012; Gibson et al., 2014; Joo et al., 2014; Lanoue et al., 2017; Li et al., 2010; Schrenk et al., 2002; Schwartz et al., 1997). Our sequencing data in Tie2-deficient PCs revealed that a great number of genes involved in neuronal and dendritic development change their expression upon loss of Tie2, indicating a complex regulatory network of downstream pathways that is affected by Tie2. In ECs, Ang1-Tie2 signaling activates the PI3K/Akt pathway that subsequently regulates mTOR activity (Kim et al., 2000; Wang et al., 2015). TSC2, mTOR, and Raptor are described to regulate PC dendritic development (Angliker et al., 2015; Reith et al., 2013; Thomanetz et al., 2013). Notably, expression of these genes was reduced in PCs of Pcp2Cre;Tie2$^{flox/flox}$ animals, supporting the hypothesis that Tie2-signaling might also affect this pathway, in PCs similar to its role in ECs.

Consistent with the requirement of a precise and controlled Tie2 activation in PCs, mice with neural-specific deletion of Ang1 or Ang2-null mice presented similar PC dendritic defects as the ones observed in mice with PC-specific deletion of Tie2. As mild vascular changes were present upon homozygous disruption of ligand expression, it cannot be completely ruled out that the vasculature contributes to the PC dendritic arborization defects in those animals. However, the fact that heterozygous mice show reduced PC dendritic complexity but no obvious vascular impairment as well as the phenotype of the PC-specific knockout of Tie2 points toward a cell-autonomous mechanism and suggest that the observed phenotypes in Ang1 and Ang2-transgenic mice are (at least in part) mediated by the lack of direct signaling to PC-Tie2. Whether other mechanisms could be altered upon lack of Ang1 or Ang2 (e.g., differential angiocrine signaling from ECs) requires further investigation.

While certain molecules are known to regulate dendritic branching, they do not regulate self-avoidance mechanisms and vice versa (Gibson et al., 2014; Kaneko et al., 2011; Kuwako and Okano, 2018). In this respect, molecular regulation of dendritic self-avoidance and planarity in PCs is incompletely understood. Here, we find that, while the absence of neural-derived Ang1, or the complete absence of Ang2, change the degree of PCs self-avoidance, PCs with specific deletion of Tie2 do not show any defects. Two models could explain these phenotypes: (1) Tie2 in PCs is required for proper self-avoidance but its deletion activates compensatory mechanisms that compensate the phenotype. Alternatively, (2) Tie2 is only required for dendritic branching but not for self-avoidance. If so, the latter would imply that Ang1/Ang2 might act on PCs to regulate self-avoidance perhaps by binding another receptor such as integrins, or that Ang1/Ang2 act on the vasculature, which in turn (either as a physical barrier or via direct signaling) affects PC dendritic self-avoidance. Further studies will be needed to elucidate these different possibilities.

The changes in PCs dendrite morphogenesis upon loss of Tie2 were accompanied by an increase in distal spine density. Consistent with increased spine density, mEPSC frequency was also increased in PCs of Pcp2Cre;Tie2$^{flox/flox}$mice. Interestingly, cumulative synapse formation has been shown to inhibit dendritic growth (Takeo et al., 2021). Thus, it is possible that the decrease in dendritic complexity could be partially due to an increase in synapse number. Whether these defects are also reflected at a behavioral level remains to be determined.

Notably, perinatal hypoxia in mice has been associated with reduced PC dendritic arborization (Ramani et al., 2013; Sathyanesan et al., 2018; Scheuer et al., 2018). As changes in oxygen level strongly affected angiopoietin expression (Abdulmalek et al., 2001; Gustavsson et al., 2007; Lin et al., 2000), it is tempting to hypothesize that changes in physiological oxygen concentrations during cerebellar development, or in pathological conditions, regulate angiopoietin expression. This might represent a mechanism adapting PC dendritic growth and branching as well as cerebellar vascular development to the environmental conditions.

STAR★METHODS

RESOURCE AVAILABILITY

Lead contact—Further information and requests for resources and reagents should be directed to and will be fulfilled by the lead contact, Carmen Ruiz de Almodóvar (carmen.ruizdealmodovar@medma.uni-heidelberg.de).

Materials availability—All unique reagents generated in this study are listed in the Key resource table and available from the lead contact with a completed Materials Transfer Agreement.

Data and code availability

- This paper also analyzes existing, publicly available data (scRNaseq). The accession number for the dataset is listed in the Key resource table.
- RNaseq FASTQ files generated in this study are available at the Gene Expression Omnibus (GEO) repository (accession number GSE178659).
- All original code is available in this paper's supplemental information
- Any additional information required to reanalyze the data reported in this paper is available from the lead contact upon request.

EXPERIMENTAL MODEL AND SUBJECT DETAILS

Cell lines—HEK293 cells were cultured in DMEM medium, supplemented with 10% v/v of fetal bovine serum (FBS), 1% l-glutamine, penicillin (100 IU mL^{-1}), and streptomycin (100 mg mL^{-1}). Cell were grown at 37°C.

Animals—The animal welfare officers and the local authorities approved all animal experiments performed in this study (G47/16, G118/16, I19/13, T38/19, T48/18, T36/17,

T46/16 and T49/15). Wild-type (CD1 or C57BL/6) animals were purchased from Janvier Labs and Charles Rivers. Transgenic animals were kept and bred in the local IBF facility of the University Heidelberg. $Ang1^{flox/flox}$ animals were previously described (Jeansson et al., 2011) and kindly provided by Susan E Quaggin. $Ang1^{flox/flox}$ mice were crossed with Nestin-Cre mice (Tronche et al., 1999). $Ang2^{-/-}$ and $Tie2^{flox/flox}$ animals were bred and used as previously described (Hu et al., 2014; Savant et al., 2015). Pcp2Cre mice (Barski et al., 2000) were kindly provided by Jaroslaw J Barski. $Rpl22^{HA/HA}$ and Rosa26:mTomato-mGFP animals (Muzumdar et al., 2007) were obtained from Jackson Laboratories. Tie2-GFP mice were described previously (De Palma et al., 2005).

Animal models in this study are listed in Key resource table. Wild-type (CD1 or C57BL/6) animals were purchased from Janvier Labs and Charls Rivers. Transgenic animals were kept and bread in the local IBF facility of the University Heidelberg. Animals were fed at the condition of 25°C and 55% of humidity and approved by the Institutional Animal Care and Use Committee of Heidelberg University. All animal experiments were performed in compliance with all institutional and national guidelines. Both sexes were used in the experiments and randomly assigned to experimental groups. In this study mice were used until 6 months of age. The specific stages are indicated in the Figures.

METHOD DETAILS

Virus production, intracranial viral injections into the cerebellum—AAV8-YFP production: to produce AAV8-YFP, a triple-plasmid transfection protocol using polyethylenimine, purification by cesium chloride density gradient centrifugation and titration by quantitative real-time PCR were used, as previously reported (Fakhiri et al., 2019). Intracranial injection of viruses was performed in pups (P7) and adults (> 6 weeks). Animals were anaesthetized using isoflurane (anesthesia initiation − 3%−2.5%; later − 2.5% −2.0%). Once the animal was deeply anaesthetized, the head was fixed in a stereotaxic device. The skin was shaved, numbed using lidocain spray (10% solution) and disinfected with 70% ethanol. A small incision was made into the skin above the cerebellum. Lambda (posterior fontanelle) was used as reference point for the injection coordinates (A/P −1.8 to −2mm; M/L 0mm; D/V −1.8 to −2mm). 500nl (pups) or 800nl (adults) of AAV8-YFP at a concentration of $1.6*10^{10}$ viral particles per ml were injected at a rate of 200nl/min using a micro injector and a Hamilton pipette. Virus was provided by Dirk Grimm (Center for Infectious Diseases; Heidelberg University). For pups, the incision of the skin was closed using 3M Vetbond Tissue Adhesive, whereby the wound of adult animal was sutured. The mice were kept on a heat plate (37°C) until they woke up and then placed back into the home cage. Animals were under continuous observation.

Tissue processing—Animals were intraperitoneally injected with ketamin/xylazin (70mg/kgBW /7mg/kgBW). Transcardial perfusion was performed for 5 min with PBS followed by 5min with 4% PFA solution. The brain was post-fixed with 4% PFA solution over night at 4°C and subsequently washed with PBS. Tissue for later cryo-sectioning was equilibrated in 30% sucrose solution (in PBS) prior embedding in Tissue-Tek® O.C.T. Compound and freezing in liquid nitrogen. PBS and PFA solutions used for ISH were previously treated with DEPC (0.1% prior autoclaving).

In situ* hybridization—In situ* hybridization (ISH) was performed on cryo-sections to localize mRNA in mouse brain tissue. Cryo-sections were hybridized with digoxigenin (DIG)-labeled antisense riboprobes (see Key resource table) in ISH hybridization buffer at a concentration of 500ng/ml. Riboprobes of the respective sense sequence were used as negative control. Hybridization was carried out o/n at 68°C. Sections were washed first with 1x SSC buffer containing 50% formamide and 0.1% Tween®20 and subsequently with 1x MAB containing 0.1% Tween®20. Sections were blocked with 2% DIG Blocking Reagent solution before applying anti-DIG antibody coupled to alkaline phosphatase 2h at RT (dilution 1:500). Subsequently, the sections were washed again with 1x MAB containing 0.1% Tween®20. Nitroblue tetrazolium/5-bromo/4-chloro-3-indolyl phosphate (NBT/BCIP concentrated at 340µg/ml and 175µg/ml ISH staining buffer) was used as chromogenic substrate. The reaction was stopped by washing with water and sections were post-fixed for 30min with 4% PFA. In case of a subsequent immunofluorescent staining the protocol described below was followed.

Immunofluorescent staining—Sagittal tissue sections were prepared using a vibratome (100µm thick slices, if not stated different) or cryostat (20µm thick slices, if not stated different). Primary and secondary antibodies used for immunofluorescent staining are listed in the key resource table. Dilutions are indicated. Briefly, sections were blocked 1h at RT in blocking solution (PBS, 1% BSA, 2% serum (depending on secondary combination) and 0.5% Triton X-100). Primary and secondary antibodies were applied in staining solution (PBS, 1% BSA, 2% serum (depending on secondary combination) and 0.3% Triton X-100). Primary antibodies were incubated at 4°C for 24h (20µm cryo-sections) or 48h (free-floating 100µm vibratome sections), respectively. Secondary antibodies were incubated at RT for 2h (20µm cryo-sections) or at 4°C for 24h (free-floating 100µm vibratome sections), respectively.

Golgi staining—Brain tissue was incubated in Golgi staining solution (1% potassium dichromate, 1% mercury chloride, 0.8% potassium chromate) for 2 days at 37°C before changing the solution to 30% sucrose in water. Sections of 250 µm were cut at the vibratome and stored in 6% sucrose in water. Sections were incubated in 15% ammonia solution for 30 min to develop Golgi reaction. Subsequently, tissue was washed with 5% sodium thiosulfate solution, dehydrated and mounted using Eukitt® medium.

Organotypic cerebellar slice cultures—Organotypic cerebellar slice cultures were prepared from P6 WT pups (for rAng1 stimulation to analyze dendritic branching) and from P13 in the case of Pcp2Cre;Rpl22$^{HA/HA}$ and Pcp2Cre;Tie2$^{flox/flox}$;Rpl22$^{HA/HA}$ animals. To prepare slices pups were sacrificed through decapitation and the brain was isolated in ice-cold dissection medium (BME; 0.45% glucose; 50mg/ml BSA; 2x glutamine; 1× ITS; 1× Penicillin/Streptomycin). The cerebellum was dissected and the meninges were removed. Cerebellar slices of 350µm were prepared using a McIlwain Tissue Chopper. Slices were transferred onto Millicells and cultured. For morphological analysis, cultures were stimulated with 100ng/ml rAng1 (R&D Systems; 923-AN) over the course of 3 days (half of the medium was replaced after 2 DIV and Ang1 stimulation was renewed). Experiment was stopped by adding warm 8% PFA containing 20% sucrose into the medium

for 1h at RT. For qPCR analysis, slices were stimulated with 100ng/ml rAng1 for 24h and subsequently snap frozen in liquid nitrogen for future processing.

Microscopy—Images of fluorescent and Golgi-staining were collected on a confocal microscope: Zeiss LSM510 unit mounted on Axiovert 200M inverted microscope; Zeiss LSM800; Nikon AR1. For Golgi-staining a reflection setting was used. ISH images were taken with stereo microscope SMZ1270i. Pictures were taken at 1024X1024 resolution using 10x, 20x or 40x objectives. Serial z stacks were taken from the scanned images. Data were saved as .lsm, .czi or .zvi file format. Digital processing of pictures was done using FIJI software (Schindelin et al., 2012).

Reconstruction and quantification of dendritic morphology—PC dendritic arbors from *in vitro* slice culture experiments (lobe V and IX; from minimum 3 independent experiments) and *in vivo* AAV-injected animals (lobe II-V from minimum 10 neurons of minimum 3 pups) were reconstructed using FIJI software plugin “Simple Neurite Tracer” (Version 3.1.6). The total length of dendrites as well as the number of dendritic branches was extracted from the .csv file. Using “Simple Neurite Tracer,” a filling of the dendritic traces was generated to clear all background and get a binary picture of the dendritic arbor.

Imaris 8.4.2 software was used to assess the number of dendritic crosses. Briefly, the binary picture of the traced dendrites was processed and skeletonized to analyze the number of loop structures, which serve as readout for dendritic self-association. These were manually counted.

Using an R language script, we analyzed PC dendritic planarity in our traced neurons. The branch endpoints were extracted from the .csv files. All points in the three two-dimensional projections (X-Y; X-Z; Y-Z) were aligned and rotated by the angle that was defined by the center of the PC-soma (first starting point in all .csv files) and the center of mass of each two-dimensional projection (see Data S1: 3DRepresentationofPurkinjecellendpoints.html file). Subsequently, the maximum width of the endpoints in the Z axis was quantified. Additionally, we wanted to visualize the distribution of endpoints in the X-Z axis. For this an ellipse containing the 95% percentile density of all branch endpoints was generated from the pooled data of control animals of each mouse line. The ellipse was fitted onto the data of all neuron from the same dataset and the percentage of branch endpoints outside the ellipse was measured (see Data S2: Ellipsoid_calculator.html file).

Quantitation of PC spines—High magnification images (63×) of PCs were taken of the AAV8-YFP injected animals used before for morphological analysis. Distal spines were manually counted using FIJI software plugin “Cell Counter” and normalized to the length.

Quantitation of blood vessel length and pericyte coverage—The length of blood vessels and the coverage of blood vessels with pericytes were analyzed in the different layers of the cerebellum using FIJI software. Pictures were taken from lobes V and IX (1–2 pictures per lobe and section; 3–5 sections per mouse). Confocal image Z stacks of blood vessels (CD31) and pericytes (CD13) were projected to a single picture with the maximum intensity. A binary picture was generated for the blood vessel and pericyte staining. Nuclear

staining of TO-PRO-3 was used to identify cerebellar layers. The signal-area of pericytes that overlaid with the blood vessel area was measured (pericyte coverage). Binary pictures of the blood vessel stain were further processed using a Gaussian Blur (sigma = 2) and auto-threshold. Particles smaller than 10 pixel were considered background and were removed. The final binary picture was processed with the FIJI plugins “Skeletonize (2D/3D)” and “Analyze Skeleton (2D/3D)” to quantify the length and number of blood vessel branches.

Rpl22$^{HA/HA}$ pull-down—The pull-down of Rpl22$^{HA/HA}$ was performed as described before (Sanz et al., 2009) using the Pcp2Cre:Rpl22$^{HA/HA}$ and Pcp2Cre:-Tie2$^{flox/flox}$:Rpl22$^{HA/HA}$ mouse lines. In short, cerebellar tissue samples were homogenized on ice in 10% w/v polysome buffer. Samples were centrifuged for 10min at 12.000rpm at 4°C, supernatant was collected and 10ml were kept as input. Remaining sample was incubated o/n at 4°C with anti-HA antibody-coated magnetic beats. Magnetic beads were washed with ice-cold HS-buffer and finally re-suspended in RLT buffer from RNeasy® Mini Kit (QIAGEN; 74104). The mRNA enrichment of PC-marker genes Pcp2 and Calbindin as well as EC-marker genes CD31 and VE-cad in the purified fraction over the input were checked to assess the quality of the pulldown (Figures 2D and 2E).

RNA sequencing and analysis—Library preparation and sequencing were performed by BGI Genomics, China. Sequencing quality check was performed with FastQC (Andrews, 2010). Mapping was performed with STAR (Dobin et al., 2013) to the mouse genome from Ensembl (Mus_musculus.GRCm38.98)(Yates et al., 2020), and the indexing with samtools (Li et al., 2009). Read counting was done using HTSeq-count (Anders et al., 2015). Differential expression analysis was done with DESeq2 (Love et al., 2014) package in R (R Team, 2020), using genotype and sequencing batch as variables. Results were obtained from the genotype differences. Data were analyzed through the use of IPA (QIAGEN Inc., https://www.qiagenbioinformatics.com/products/ingenuity-pathway-analysis) (Krämer et al., 2014). The IPA output was visualized using R scripts.

Animals and slice preparation—Mice were sent from Heidelberg according to the given guidelines of Baden-Württemberg and Rhineland-Palatinate. Before the experiments, mice were housed for at least one week in the animal housing of the BFZ of the University Medicine Mainz under a 12h/12h light/dark cycle and had access to water and food *ad libitum*.

Animals of 8–11 weeks old (aprox. postnatal days 67–79) were used in electrophysiological experiments. All mice were handled according to the guidelines of the Landesuntersuchungsamt (LUA) Rheinlandpfalz and were anesthetized with isoflurane and decapitated. Mice were transcardially perfused with ice-cold sucrose containing solution bubbled with carbogen gas using the following composition (in mM): Sucrose (212), KCl (3), NaH_2PO_4 (1.25), $MgCl_2$ (7), $CaCl_2$ (0.16), $NaHCO_3$ (26), glucose (10). The brain was quickly removed and sectioned to contain the vermis region of the cerebellum.

Sagittal slices of the vermis of the cerebellum at a thickness of 250 μm were made using a Leica VT1200S at a speed of 0.1 mm/s and 1 mm amplitude using Personna razor blades. Slices were transferred into carbogen-bubbled Ringer’s solution for 30 min at 34°C for

recovery containing (in mM): NaCl (125), $NaHCO_3$ (25), KCl (2.5), NaH_2PO_4 (1.25), $CaCl_2$ (2), $MgCl_2$ (1), glucose (25). Slices were kept at room temperature until recording.

Electrophysiology—Whole-cell voltage clamp recordings were performed at a holding potential of —70 mV in Ringer's solution containing (in mM): NaCl (125), $NaHCO_3$ (25), KCl (2.5), NaH_2PO_4 (1.25), $CaCl_2$ (2), $MgCl_2$ (1), glucose (25) and 1 mM TTX to block Na^+-channels. For mEPSC recordings, 10 μm gabazine and 50 μm APV was added to block GABA receptor- and NMDA receptor-mediated currents, respectively. For mIPSC recordings, 50 μm APV and 10 μm CNQX was added to block NMDA and AMPA mediated currents, respectively. Recording electrodes were made using borosilicate glass pipettes with a resistance of 3–5 MU when filled with intracellular recording solution containing in mM (for mEPSC recording): Cs^+-methanesulfonate (120), CsCl (10), EGTA (0.2), HEPES (10), Phosphocreatin- Na^+ (0.1), ATP-Mg^{2+} salt (2), NaCl (8), GTP (0.3) or (for mIPSC recording): CsCl (145), HEPES (10), EGTA (0.1), ATP-Mg^{2+} salt (2), $MgCl_2$ (2). Series resistance was continuously monitored by applying a +5 mV pulse at the start of each sweep. Cells exceeding 30 MΩ series resistance were omitted. All recordings were performed at room temperature using an EPC10 double USB patch clamp amplifier with Patchmaster software (HEKA Elektronic, Germany). Signals were filtered with two Bessel filters (2.9 and 10 kHz) and digitized at 20 kHz. Purkinje cells in the vermis region of the cerebellum (lobes IV-V) were visualized on an upright Olympus BX51W1 microscope with differential interference contrast (DIC) optics using a 40× water immersion objective (LUMPlanFl/IR 40× 0.80 W) and an Olympus XM10 digital camera. Miniature current analysis was performed with Clampfit software using a template matching algorithm (10.2.0.13, MDS Analytical Technologies, 2007).

Data analysis—Data was subjected to Shapiro Wilks test for normality and if normal distribution was given, a subsequent two sample t test was performed. In case of a rejected normal distribution a non-parametric Mann-Whitney test was performed using R scripts. Differences between two groups leading to p values < 0.05 were considered significant.

Electrophysiological recordings of spontaneous activity: Slice preparation—Mice, female and male, 8–11 weeks old, were decapitate under deep isoflurane anesthesia. All experiments were conducted in accordance with international guidelines from the European Community Council Directive and with the local guideline on the ethical use of animals. The cerebellum was removed and immersed into ice-cold (2–3°C) "slicing" solution containing (in mM): 240 sucrose, 5 KCl, 1.25 Na_2HPO_4, 2 $MgSO_4$, 1 $CaCl_2$, 26 $NaHCO_3$ and 10 D-Glucose, bubbled with 95% O_2 and 5% CO_2. Cerebellar vermis was isolated and parasagittal slices (220 μm thick) were cut using a vibratome (VT1200S, Leica). Slices were incubated for at least 1 h before recordings in ACSF containing (in mM): 125 NaCl, 2.5 KCl, 1.25 Na_2HPO4, 1 $MgSO_4$, 2 $CaCl_2$, 26 $NaHCO_3$ and 25 D-Glucose, bubbled with 95% O_2 and 5% CO_2, maintained at 32°C.

Electrophysiological apparatus and patch-clamp recordings—For electrophysiological recordings, slices were transferred to the recording chamber and perfused at 1.5 mL min −1 with ACSF in the presence of 100 μm picrotoxin unless stated

otherwise, bubbled with 95% O_2 and 5% CO_2, at room temperature (RT; 20–23°C). Slices were visualized with an upright microscope equipped with a × 63, 0·9 NA water-immersion objective and differential interference contrast (DIC) optics (Scientifica, UK).

Patch pipettes were made from thick-walled borosilicate glass capillaries with filament (GB150F-8P, Science Product) by means of a Sutter P-1000 horizontal puller (Sutter Instruments, Novato, CA, USA). Recordings were obtained in patch-clamp cell-attached configuration using an Axoclamp 200B amplifier (Molecular Devices, Union City, CA, USA).

For cell-attached recordings (10–80MΩseal resistance), patch pipettes were filled with standard extracellular saline. Pipettes were held at 0 mV in the voltage-clamp mode. Consecutive 140 s. current traces were filtered at 2 kHz and acquired at 50 kHz sampling rate. In these conditions, recorded spikes appear as biphasic current deflections (6M*, right inset*). Recordings were judged to be stable when the shape and frequency of spikes was constant over time (6M). Stable recordings were routinely obtained for as long as 20–30min (6M).

Data analysis—In cell-attached recordings, firing frequency (Inst. Freq.) of the tonic simple spikes was evaluated with the event-sorting function in pClamp 10 Software suite; the variability of the interspike interval (ISI) was calculated from the mean ISI and the ISI coefficient of variation (CV(ISI)) computed as standard deviation of interspike intervals (ISI)/mean of ISI . Each Freq. and CV(ISI) value was computed from an event-sample recorded over a time window of 140 s. All values are represented as mean ± s.e.m, p values of < 0.05 were considered significant. Statistical analysis was done using unpaired Student's t test, unless stated otherwise.

qRT-PCR analysis—RNA from RiboTag-tissue was isolated by using the RNeasy® Mini Kit, following manufacturer's instructions. RNA from whole cerebellum was isolated using TRIzol Reagent. RNA was DNaseI-treated and reverse-transcribed using either Maxima Reverse Transcriptase or SuperScript®Vilo. qRT-PCR was performed using Fast SYBR Green Master Mix to assess mRNA expression levels. *Gapdh* served as control for normalization. The qRT-PCR primers are listed in the key resource table.

QUANTIFICATION AND STATISTICAL ANALYSIS

Statistical analyses were performed using GraphPad Prism 6.0 software (GraphPad Software Inc.). All data are shown as mean ± SEM if not stated otherwise. The unpaired Student's t test was used for comparison between two groups, if not stated otherwise. One-way ANOVA together with Dunnett's multiple comparisons test was used for comparison between multiple groups to the same control condition. The investigator was blinded for all analysis. The experiments were not randomized and no samples were excluded from the analysis. Statistical significance was defined as $*p < 0.05$; $**p < 0.01$; $***p < 0.001$ and $****p < 0.0001$. Statistical details of the experiments can be found in the respective figure legends.

Supplementary Material

Refer to Web version on PubMed Central for supplementary material.

ACKNOWLEDGMENTS

We thank the Nikon Imaging Center, the Math-Clinic, and the INBC of the University of Heidelberg for their support. We thank Prof. Susan E. Quaggin for providing the $Ang1^{fl/fl}$ mice (supported by the National Institutes of Health (P30 DK114857 [PI-SEQ]), Prof. Barski for the Pcp2-Cre mice, and Prof. Dr. Hannah Monyer for the Nestin:Cre mice. We thank Andreas Fischer and Juan Rodriguez-Vita for their support with the IPA analysis. We thank Melanie Richter, Alberto Arenas Molina, Daniel Maeso Miguel, Philip Ruthig, and Yi Lien for technical assistance and Prof. Daniela Mauceri and the entire Ruiz de Almodovar lab for useful discussions. The authors gratefully acknowledge the data storage service SDS@hd supported by the Ministry of Science, Research and the Arts Baden-Württemberg (M.W.K.) and the German Research Foundation (DFG) through grant INST 35/1314–1 FUGG and INST 35/1503–1 FUGG. R.L. was supported by a Boehringer Ingelheim Fonds fellowship. This work was supported by the Schram Foundation and the Chica and Heinz Schaller Foundation, by research grants of the Deutsche Forschungsgemeinschaft (DFG) from FOR2325 (“Interactions at the Neurovascular Interface” [to C.R.d.A and R.H.A.]), by DFG grants from SFB1366 (“Vascular Control of Organ Function;” Project number 394046768-SFB 1366; [to C.R.d.A., R.H.A., and H.G.A.]), by funds from the Baden-Württemberg Stiftung special programme “Angioformatics Single Cell Platform” (to C.R.d.A. and to H.G.A.), and by the European Research Council Consolidator grant 864875 “OLI.VAS” (to C.R.d.A.) and ERC Advance Grant 787181 “Angiomature” (to H.G.A.).

REFERENCES

Abdulmalek K, Ashur F, Ezer N, Ye F, Magder S, and Hussain SN (2001). Differential expression of Tie-2 receptors and angiopoietins in response to in vivo hypoxia in rats. Am. J. Physiol. Lung Cell. Mol. Physiol. 281, L582–L590. [PubMed: 11504684]

Adamaszek M, D’Agata F, Ferrucci R, Habas C, Keulen S, Kirkby KC, Leggio M, Mariën P, Molinari M, Moulton E, et al. (2017). Consensus Paper: Cerebellum and Emotion. Cerebellum 16, 552–576. [PubMed: 27485952]

Anders S, Pyl PT, and Huber W. (2015). HTSeq–a Python framework to work with high-throughput sequencing data. Bioinformatics 31, 166–169. [PubMed: 25260700]

Andrews S. (2010). FastQC: A Quality Control Tool for High Throughput Sequence Data, http://www.bioinformatics.babraham.ac.uk/projects/fastqc/.

Androutsellis-Theotokis A, Rueger MA, Park DM, Mkhikian H, Korb E, Poser SW, Walbridge S, Munasinghe J, Koretsky AP, Lonser RR, and McKay RD (2009). Targeting neural precursors in the adult brain rescues injured dopamine neurons. Proc. Natl. Acad. Sci. USA 106, 13570–13575. [PubMed: 19628689]

Angliker N, Burri M, Zaichuk M, Fritschy JM, and Rüegg MA (2015). mTORC1 and mTORC2 have largely distinct functions in Purkinje cells. Eur. J. Neurosci. 42, 2595–2612. [PubMed: 26296489]

Augustin HG, Koh GY, Thurston G, and Alitalo K. (2009). Control of vascular morphogenesis and homeostasis through the angiopoietin-Tie system. Nat. Rev. Mol. Cell Biol. 10, 165–177. [PubMed: 19234476]

Bai Y, Cui M, Meng Z, Shen L, He Q, Zhang X, Chen F, and Xiao J. (2009). Ectopic expression of angiopoietin-1 promotes neuronal differentiation in neural progenitor cells through the Akt pathway. Biochem. Biophys. Res. Commun. 378, 296–301. [PubMed: 19028450]

Baldwin ME, Catimel B, Nice EC, Roufail S, Hall NE, Stenvers KL, Karkkainen MJ, Alitalo K, Stacker SA, and Achen MG (2001). The specificity of receptor binding by vascular endothelial growth factor-d is different in mouse and man. J. Biol. Chem. 276, 19166–19171. [PubMed: 11279005]

Barski JJ, Dethleffsen K, and Meyer M. (2000). Cre recombinase expression in cerebellar Purkinje cells. Genesis 28, 93–98. [PubMed: 11105049]

Buffo A, and Rossi F. (2013). Origin, lineage and function of cerebellar glia. Prog. Neurobiol. 109, 42–63. [PubMed: 23981535]

Butts T, Green MJ, and Wingate RJ (2014). Development of the cerebellum: simple steps to make a 'little brain'. Development 141, 4031–4041. [PubMed: 25336734]

Carter RA, Bihannic L, Rosencrance C, Hadley JL, Tong Y, Phoenix TN, Natarajan S, Easton J, Northcott PA, and Gawad C. (2018). A Single-Cell Transcriptional Atlas of the Developing Murine Cerebellum. Curr. Biol. 28, 2910–2920.e2. [PubMed: 30220501]

D'Angelo E, Mazzarello P, Prestori F, Mapelli J, Solinas S, Lombardo P, Cesana E, Gandolfi D, and Congi L. (2011). The cerebellar network: from structure to function and dynamics. Brain Res. Brain Res. Rev. 66, 5–15.

De Palma M, Venneri MA, Galli R, Sergi Sergi L, Politi LS, Sampaolesi M, and Naldini L. (2005). Tie2 identifies a hematopoietic lineage of proangiogenic monocytes required for tumor vessel formation and a mesenchymal population of pericyte progenitors. Cancer Cell 8, 211–226. [PubMed: 16169466]

Dobin A, Davis CA, Schlesinger F, Drenkow J, Zaleski C, Jha S, Batut P, Chaisson M, and Gingeras TR (2013). STAR: ultrafast universal RNA-seq aligner. Bioinformatics 29, 15–21. [PubMed: 23104886]

Fakhiri J, Schneider MA, Puschhof J, Stanifer M, Schildgen V, Holderbach S, Voss Y, El Andari J, Schildgen O, Boulant S, et al. (2019). Novel Chimeric Gene Therapy Vectors Based on Adeno-Associated Virus and Four Different Mammalian Bocaviruses. Mol. Ther. Methods Clin. Dev. 12, 202–222. [PubMed: 30766894]

Fiedler U, Reiss Y, Scharpfenecker M, Grunow V, Koidl S, Thurston G, Gale NW, Witzenrath M, Rosseau S, Suttorp N, et al. (2006). Angiopoietin-2 sensitizes endothelial cells to TNF-alpha and has a crucial role in the induction of inflammation. Nat. Med. 12, 235–239. [PubMed: 16462802]

Fleming JT, He W, Hao C, Ketova T, Pan FC, Wright CCV, Litingtung Y, and Chiang C. (2013). The Purkinje neuron acts as a central regulator of spatially and functionally distinct cerebellar precursors. Dev. Cell 27, 278–292. [PubMed: 24229643]

Fujishima K, Horie R, Mochizuki A, and Kengaku M. (2012). Principles of branch dynamics governing shape characteristics of cerebellar Purkinje cell dendrites. Development 139, 3442–3455. [PubMed: 22912417]

Gale NW, Thurston G, Hackett SF, Renard R, Wang Q, McClain J, Martin C, Witte C, Witte MH, Jackson D, et al. (2002). Angiopoietin-2 is required for postnatal angiogenesis and lymphatic patterning, and only the latter role is rescued by Angiopoietin-1. Dev. Cell 3, 411–423. [PubMed: 12361603]

Gibson DA, Tymanskyj S, Yuan RC, Leung HC, Lefebvre JL, Sanes JR, Cheódotal A, and Ma L. (2014). Dendrite self-avoidance requires cell-autonomous slit/robo signaling in cerebellar purkinje cells. Neuron 81, 1040–1056. [PubMed: 24607227]

Gustavsson M, Mallard C, Vannucci SJ, Wilson MA, Johnston MV, and Hagberg H. (2007). Vascular response to hypoxic preconditioning in the immature brain. J. Cereb. Blood Flow Metab. 27, 928–938. [PubMed: 17033689]

Hansen TM, Singh H, Tahir TA, and Brindle NP (2010). Effects of angiopoietins-1 and −2 on the receptor tyrosine kinase Tie2 are differentially regulated at the endothelial cell surface. Cell. Signal. 22, 527–532. [PubMed: 19922791]

Heuer H, and Mason CA (2003). Thyroid hormone induces cerebellar Purkinje cell dendritic development via the thyroid hormone receptor alpha1. J. Neurosci. 23, 10604–10612. [PubMed: 14627645]

Hu J, Srivastava K, Wieland M, Runge A, Mogler C, Besemfelder E, Terhardt D, Vogel MJ, Cao L, Korn C, et al. (2014). Endothelial cell-derived angiopoietin-2 controls liver regeneration as a spatiotemporal rheostat. Science 343, 416–419. [PubMed: 24458641]

Huang GJ, Edwards A, Tsai CY, Lee YS, Peng L, Era T, Hirabayashi Y, Tsai CY, Nishikawa S, Iwakura Y, et al. (2014). Ectopic cerebellar cell migration causes maldevelopment of Purkinje cells and abnormal motor behaviour in Cxcr4 null mice. PLoS ONE 9, e86471.

Ing-Esteves S, Kostadinov D, Marocha J, Sing AD, Joseph KS, Laboulaye MA, Sanes JR, and Lefebvre JL (2018). Combinatorial Effects of Alpha- and Gamma-Protocadherins on Neuronal Survival and Dendritic Self-Avoidance. J. Neurosci. 38, 2713–2729. [PubMed: 29439167]

Jeansson M, Gawlik A, Anderson G, Li C, Kerjaschki D, Henkelman M, and Quaggin SE (2011). Angiopoietin-1 is essential in mouse vasculature during development and in response to injury. J. Clin. Invest. 121, 2278–2289. [PubMed: 21606590]

Joo W, Hippenmeyer S, and Luo L. (2014). Neurodevelopment. Dendrite morphogenesis depends on relative levels of NT-3/TrkC signaling. Science 346, 626–629. [PubMed: 25359972]

Kaneko M, Yamaguchi K, Eiraku M, Sato M, Takata N, Kiyohara Y, Mishina M, Hirase H, Hashikawa T, and Kengaku M. (2011). Remodeling of monoplanar Purkinje cell dendrites during cerebellar circuit formation. PLoS ONE 6, e20108.

Kawabata Galbraith K, Fujishima K, Mizuno H, Lee SJ, Uemura T, Sakimura K, Mishina M, Watanabe N, and Kengaku M. (2018). MTSS1 Regulation of Actin-Nucleating Formin DAAM1 in Dendritic Filopodia Determines Final Dendritic Configuration of Purkinje Cells. Cell Rep. 24, 95–106.e9. [PubMed: 29972794]

Kim I, Kim HG, So JN, Kim JH, Kwak HJ, and Koh GY (2000). Angiopoietin-1 regulates endothelial cell survival through the phosphatidylinositol 3′-Kinase/Akt signal transduction pathway. Circ. Res. 86, 24–29. [PubMed: 10625301]

Kosacka J, Figiel M, Engele J, Hilbig H, Majewski M, and Spanel-Borowski K. (2005). Angiopoietin-1 promotes neurite outgrowth from dorsal root ganglion cells positive for Tie-2 receptor. Cell Tissue Res. 320, 11–19. [PubMed: 15714275]

Koziol LF, Budding D, Andreasen N, D'Arrigo S, Bulgheroni S, Imamizu H, Ito M, Manto M, Marvel C, Parker K, et al. (2014). Consensus paper: the cerebellum's role in movement and cognition. Cerebellum 13, 151–177. [PubMed: 23996631]

Krämer A, Green J, Pollard J Jr., and Tugendreich S. (2014). Causal analysis approaches in Ingenuity Pathway Analysis. Bioinformatics 30, 523–530. [PubMed: 24336805]

Kuwako KI, and Okano H. (2018). The LKB1-SIK Pathway Controls Dendrite Self-Avoidance in Purkinje Cells. Cell Rep. 24, 2808–2818.e4. [PubMed: 30208308]

Lanoue V, Langford M, White A, Sempert K, Fogg L, and Cooper HM (2017). The Wnt receptor Ryk is a negative regulator of mammalian dendrite morphogenesis. Sci. Rep. 7, 5965. [PubMed: 28729735]

Lefebvre JL, Kostadinov D, Chen WV, Maniatis T, and Sanes JR (2012). Protocadherins mediate dendritic self-avoidance in the mammalian nervous system. Nature 488, 517–521. [PubMed: 22842903]

Leto K, Arancillo M, Becker EB, Buffo A, Chiang C, Ding B, Dobyns WB, Dusart I, Haldipur P, Hatten ME, et al. (2016). Consensus Paper: Cerebellar Development. Cerebellum 15, 789–828. [PubMed: 26439486]

Li H, Handsaker B, Wysoker A, Fennell T, Ruan J, Homer N, Marth G, Abecasis G, and Durbin R; 1000 Genome Project Data Processing Sub-group (2009). The Sequence Alignment/Map format and SAMtools. Bioinformatics 25, 2078–2079.

Li J, Gu X, Ma Y, Calicchio ML, Kong D, Teng YD, Yu L, Crain AM, Vartanian TK, Pasqualini R, et al. (2010). Nna1 mediates Purkinje cell dendritic development via lysyl oxidase propeptide and NF-kB signaling. Neuron 68, 45–60. [PubMed: 20920790]

Lin TN, Wang CK, Cheung WM, and Hsu CY (2000). Induction of angiopoietin and Tie receptor mRNA expression after cerebral ischemia-reperfusion. J. Cereb. Blood Flow Metab. 20, 387–395. [PubMed: 10698077]

Liu XS, Chopp M, Zhang RL, Hozeska-Solgot A, Gregg SC, Buller B, Lu M, and Zhang ZG (2009). Angiopoietin 2 mediates the differentiation and migration of neural progenitor cells in the subventricular zone after stroke. J. Biol. Chem. 284, 22680–22689. [PubMed: 19553662]

Love MI, Huber W, and Anders S. (2014). Moderated estimation of fold change and dispersion for RNA-seq data with DESeq2. Genome Biol. 15, 550. [PubMed: 25516281]

Maricich SM, and Herrup K. (1999). Pax-2 expression defines a subset of GABAergic interneurons and their precursors in the developing murine cerebellum. J. Neurobiol. 41, 281–294. [PubMed: 10512984]

Marteau L, Pacary E, Valable S, Bernaudin M, Guillemot F, and Petit E. (2011). Angiopoietin-2 regulates cortical neurogenesis in the developing telencephalon. Cereb. Cortex 21, 1695–1702. [PubMed: 21127017]

McKay BE, and Turner RW (2005). Physiological and morphological development of the rat cerebellar Purkinje cell. J. Physiol. 567, 829–850. [PubMed: 16002452]

Michinaga S, Tanabe A, Nakaya R, Fukutome C, Inoue A, Iwane A, Minato Y, Tujiuchi Y, Miyake D, Mizuguchi H, et al. (2020). Angiopoietin-1/Tie-2 signal after focal traumatic brain injury is potentiated by BQ788, an ETB receptor antagonist, in the mouse cerebrum: Involvement in recovery of blood-brain barrier function. J. Neurochem. 154, 330–348. [PubMed: 31957020]

Muzumdar MD, Tasic B, Miyamichi K, Li L, and Luo L. (2007). A global double-fluorescent Cre reporter mouse. Genesis 45, 593–605. [PubMed: 17868096]

Parati EA, Bez A, Ponti D, de Grazia U, Corsini E, Cova L, Sala S, Colombo A, Alessandri G, and Pagano SF (2002). Human neural stem cells express extra-neural markers. Brain Res. 925, 213–221. [PubMed: 11792370]

Paredes I, Himmels P, and Ruiz de Almodóvar C. (2018). Neurovascular Communication during CNS Development. Dev. Cell 45, 10–32. [PubMed: 29634931]

Ramani M, van Groen T, Kadish I, Bulger A, and Ambalavanan N. (2013). Neurodevelopmental impairment following neonatal hyperoxia in the mouse. Neurobiol. Dis. 50, 69–75. [PubMed: 23064437]

Reith RM, McKenna J, Wu H, Hashmi SS, Cho SH, Dash PK, and Gambello MJ (2013). Loss of Tsc2 in Purkinje cells is associated with autistic-like behavior in a mouse model of tuberous sclerosis complex. Neuro biol. Dis. 51, 93–103.

Rosa AI, Gonçalves J, Cortes L, Bernardino L, Malva JO, and Agasse F. (2010). The angiogenic factor angiopoietin-1 is a proneurogenic peptide on subventricular zone stem/progenitor cells. J. Neurosci. 30, 4573–4584. [PubMed: 20357108]

Sanz E, Yang L, Su T, Morris DR, McKnight GS, and Amieux PS (2009). Cell-type-specific isolation of ribosome-associated mRNA from complex tissues. Proc. Natl. Acad. Sci. USA 106, 13939–13944. [PubMed: 19666516]

Sathyanesan A, Kundu S, Abbah J, and Gallo V. (2018). Neonatal brain injury causes cerebellar learning deficits and Purkinje cell dysfunction. Nat. Commun. 9, 3235. [PubMed: 30104642]

Savant S, La Porta S, Budnik A, Busch K, Hu J, Tisch N, Korn C, Valls AF, Benest AV, Terhardt D, et al. (2015). The Orphan Receptor Tie1 Controls Angiogenesis and Vascular Remodeling by Differentially Regulating Tie2 in Tip and Stalk Cells. Cell Rep. 12, 1761–1773. [PubMed: 26344773]

Scheuer T, Sharkovska Y, Tarabykin V, Marggraf K, Brockmöller V, Bührer C, Endesfelder S, and Schmitz T. (2018). Neonatal Hyperoxia Perturbs Neuronal Development in the Cerebellum. Mol. Neurobiol. 55, 3901–3915. [PubMed: 28547531]

Schindelin J, Arganda-Carreras I, Frise E, Kaynig V, Longair M, Pietzsch T, Preibisch S, Rueden C, Saalfeld S, Schmid B, et al. (2012). Fiji: an open-source platform for biological-image analysis. Nat. Methods 9, 676–682. [PubMed: 22743772]

Schrenk K, Kapfhammer JP, and Metzger F. (2002). Altered dendritic development of cerebellar Purkinje cells in slice cultures from protein kinase Cgamma-deficient mice. Neuroscience 110, 675–689. [PubMed: 11934475]

Schwartz PM, Borghesani PR, Levy RL, Pomeroy SL, and Segal RA (1997). Abnormal cerebellar development and foliation in BDNF−/− mice reveals a role for neurotrophins in CNS patterning. Neuron 19, 269–281. [PubMed: 9292718]

Segarra M, Aburto MR, Hefendehl J, and Acker-Palmer A. (2019). Neurovascular Interactions in the Nervous System. Annu. Rev. Cell Dev. Biol. 35, 615–635. [PubMed: 31590587]

Takeo YH, Kakegawa W, Miura E, and Yuzaki M. (2015). RORα Regulates Multiple Aspects of Dendrite Development in Cerebellar Purkinje Cells In Vivo. J. Neurosci. 35, 12518–12534. [PubMed: 26354918]

Takeo YH, Shuster SA, Jiang L, Hu MC, Luginbuhl DJ, Rülicke T, Contreras X, Hippenmeyer S, Wagner MJ, Ganguli S, and Luo L. (2021). GluD2- and Cbln1-mediated competitive interactions shape the dendritic arbors of cerebellar Purkinje cells. Neuron 109, 629–644.e8. [PubMed: 33352118]

R Team (2020). R: A language and environment for statistical computing (R Foundation for Statistical Computing).

Teichert M, Milde L, Holm A, Stanicek L, Gengenbacher N, Savant S, Ruckdeschel T, Hasanov Z, Srivastava K, Hu J, et al. (2017). Pericyte-expressed Tie2 controls angiogenesis and vessel maturation. Nat. Commun. 8, 16106. [PubMed: 28719590]

Thomanetz V, Angliker N, Cloëtta D, Lustenberger RM, Schweighauser M, Oliveri F, Suzuki N, and Ru€egg MA (2013). Ablation of the mTORC2 component rictor in brain or Purkinje cells affects size and neuron morphology. J. Cell Biol. 201, 293–308. [PubMed: 23569215]

Toyoda S, Kawaguchi M, Kobayashi T, Tarusawa E, Toyama T, Okano M, Oda M, Nakauchi H, Yoshimura Y, Sanbo M, et al. (2014). Developmental epigenetic modification regulates stochastic expression of clustered protocadherin genes, generating single neuron diversity. Neuron 82, 94–108. [PubMed: 24698270]

Tronche F, Kellendonk C, Kretz O, Gass P, Anlag K, Orban PC, Bock R, Klein R, and Schütz G. (1999). Disruption of the glucocorticoid receptor gene in the nervous system results in reduced anxiety. Nat. Genet. 23, 99–103. [PubMed: 10471508]

Venneri MA, De Palma M, Ponzoni M, Pucci F, Scielzo C, Zonari E, Mazzieri R, Doglioni C, and Naldini L. (2007). Identification of proangiogenic TIE2-expressing monocytes (TEMs) in human peripheral blood and cancer. Blood 109, 5276–5285. [PubMed: 17327411]

Wang VY, and Zoghbi HY (2001). Genetic regulation of cerebellar development. Nat. Rev. Neurosci. 2, 484–491. [PubMed: 11433373]

Wang S, Amato KR, Song W, Youngblood V, Lee K, Boothby M, Brantley-Sieders DM, and Chen J. (2015). Regulation of endothelial cell proliferation and vascular assembly through distinct mTORC2 signaling pathways. Mol. Cell. Biol. 35, 1299–1313. [PubMed: 25582201]

Ward NL, Putoczki T, Mearow K, Ivanco TL, and Dumont DJ (2005). Vascular-specific growth factor angiopoietin 1 is involved in the organization of neuronal processes. J. Comp. Neurol. 482, 244–256. [PubMed: 15690488]

Wojcinski A, Lawton AK, Bayin NS, Lao Z, Stephen DN, and Joyner AL (2017). Cerebellar granule cell replenishment postinjury by adaptive reprogramming of Nestin+ progenitors. Nat. Neurosci. 20, 1361–1370. [PubMed: 28805814]

Yates AD, Achuthan P, Akanni W, Allen J, Allen J, Alvarez-Jarreta J, Amode MR, Armean IM, Azov AG, Bennett R, et al. (2020). Ensembl 2020. Nucleic Acids Res. 48 (D1), D682–D688. [PubMed: 31691826]

Zhang B, Chen LY, Liu X, Maxeiner S, Lee SJ, Gokce O, and Südhof TC (2015). Neuroligins Sculpt Cerebellar Purkinje-Cell Circuits by Differential Control of Distinct Classes of Synapses. Neuron 87, 781–796. [PubMed: 26291161]

Highlights

- Ang1 and Ang2 are expressed in cerebellar neural and endothelial cells, respectively
- The angiopoietin receptor Tie2 is expressed in blood vessels and Purkinje cells
- Tie2 signaling regulates PC dendritic morphogenesis in a cell-autonomous manner
- PCs network functionality is altered in PC specific Tie2-deficient mice

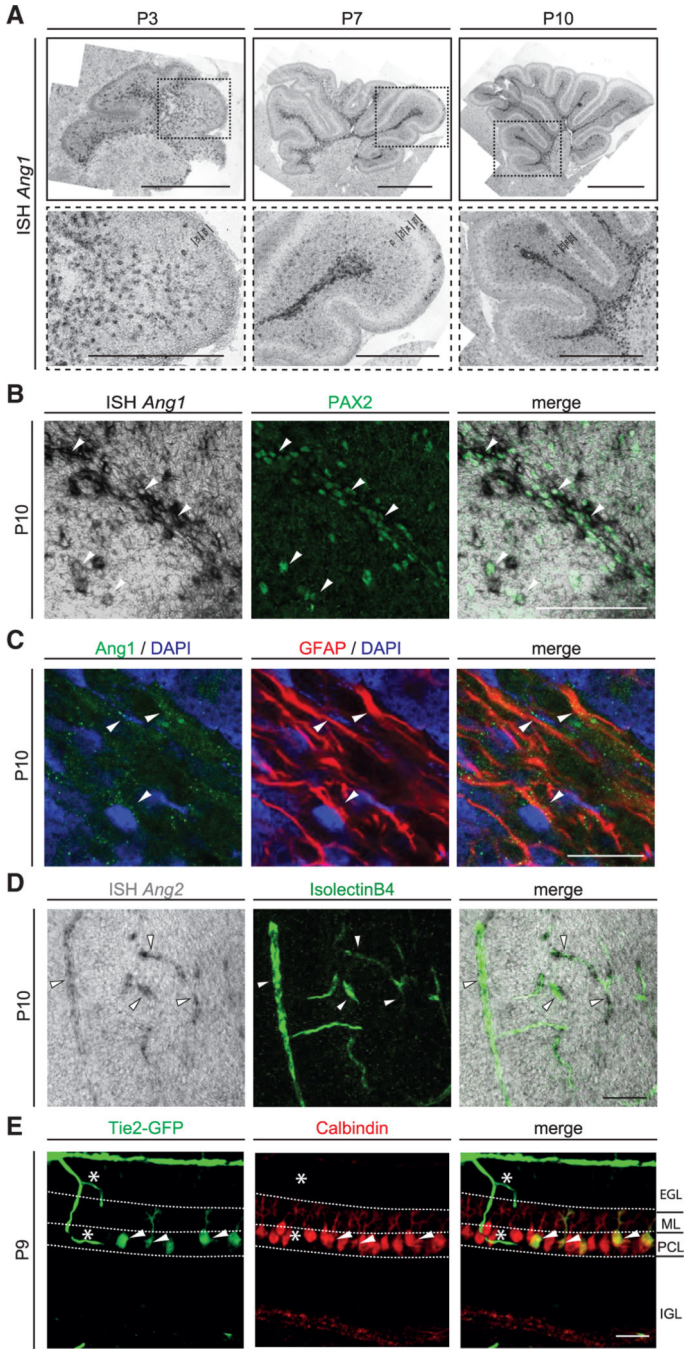

Figure 1. Ang1, Ang2, and Tie2 are expressed by distinct cell types during development of the cerebellum

(A) ISH of *Ang1* mRNA in sections of cerebellum at different postnatal stages. Bottom images show insets of the respective top image. Scale bar, 1 mm (overview) and 500 μm (higher magnification).

(B) ISH of *Ang1* mRNA on P10 cerebellar tissue together with IF staining of GABAergic interneuron lineage marker PAX2.

(C) IF staining of Ang1 on P10 cerebellar tissue together with astrocyte marker GFAP and DAPI.

(D) ISH of *Ang2* mRNA on P10 cerebellar tissue combined with IsolectinB4 (EC marker). (E) Representative image of cerebellar tissue of P9 Tie2-GFP mice stained for GFP and Calbindin (PC marker).

Double-positive cells are indicated with white arrowhead in (B)–(E). Asterisks shows GFP-positive blood vessels in (E). Scale bar in (B): 100 μm, (C): 20 μm and in (D) and (E): 50 μm. See also Figure S1.

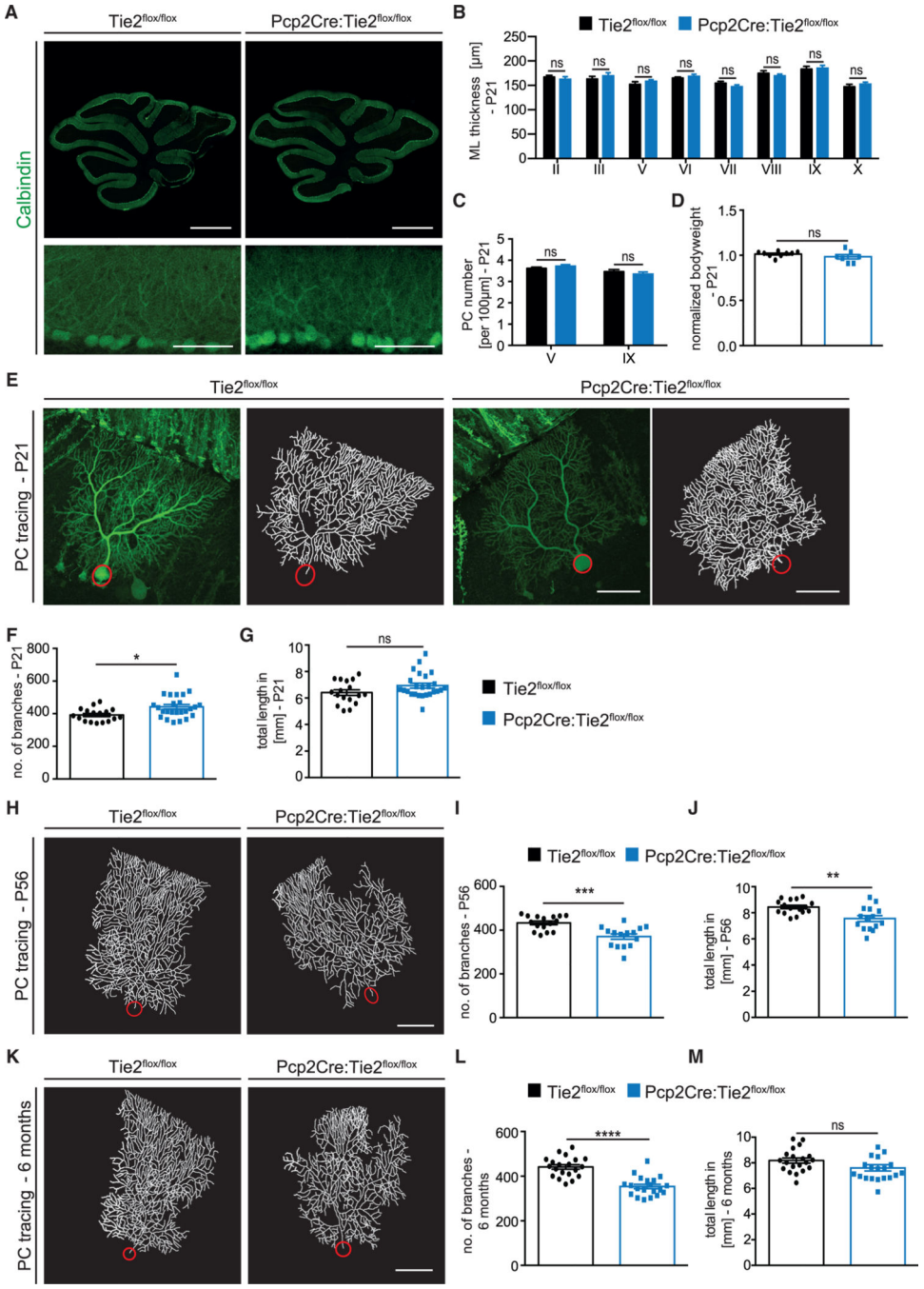

Figure 2. PC-specific deletion of Tie2 leads to a progressive reduction in PC dendritic complexity

(A) Representative images of P21 Tie2$^{flox/flox}$ and Pcp2Cre:Tie2$^{flox/flox}$ cerebella stained with Calbindin. Scale bar, 1 mm (top panels) and 100 µm (bottom panels).

(B) Bar graph showing ML thickness at P21 in all cerebella lobes (II-X).

(C) Bar graph showing PC number per 100 µm in lobes V and IX. Data in (B) and (C) are shown as mean ± SEM from minimum n = 7 animals per genotype.

(D) Bar graph showing normalized bodyweight of Tie2$^{flox/flox}$ and Pcp2Cre:Tie2$^{flox/flox}$ P21 mice. Data are shown as mean ± SEM from a minimum of n = 7 animals.

(E) Representative images of PCs from P21 Tie2$^{flox/flox}$ and Pcp2Cre:Tie2$^{flox/flox}$ mice labeled with YFP using AAV8 (left panels) and corresponding tracing (right panels).
(F and G) Quantitation of the number of branches (F) and total dendritic length (G) at P21.
(H) Representative image of traced PCs of Tie2$^{flox/flox}$ and Pcp2Cre:Tie2$^{flox/flox}$ mice at P56.
(I and J) Quantitation of the number of branches (I) and total dendritic length (J) at P56.
K) Representative image of traced PCs of Tie2$^{flox/flox}$ and Pcp2Cre: Tie2$^{flox/flox}$ mice at 6 months.
(L and M) Quantitation of the number of branches (L) and total dendritic length (M) at 6 months.
Data in (E)–(M) are shown as mean ± SEM from a minimum of n = 15 neurons of a minimum of 3 independent animals. Unpaired Student's t test; *p < 0.05; **p < 0.01; ***p < 0.001; ****p < 0.0001; ns = not significant. Scale bar in (E), (H), and (K), 50 μm. See also Figures S3, S4, and S6.

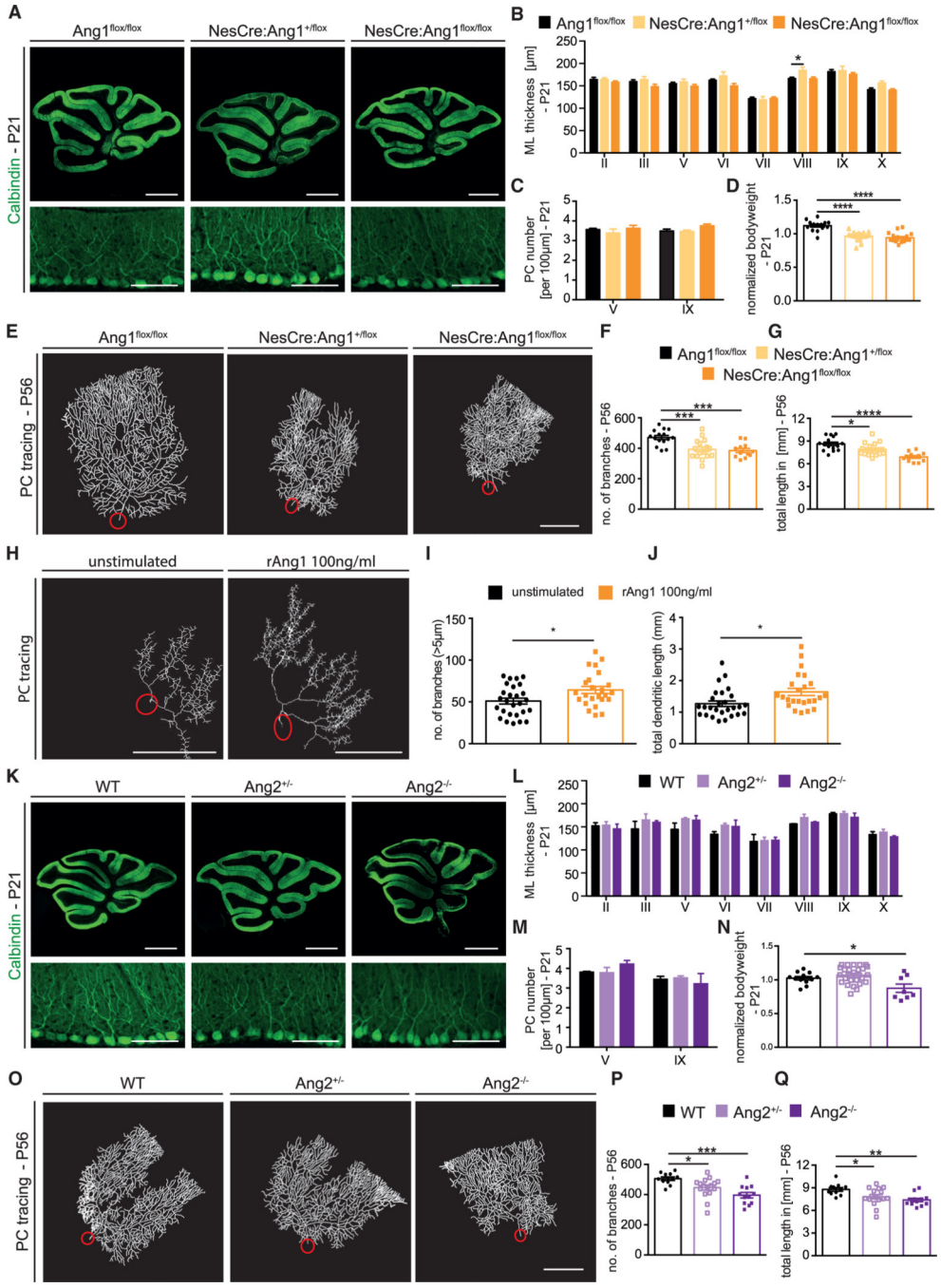

Figure 3. Mice with neural-specific deletion of Ang1 or Ang2 full knockout mice present aberrant PC dendritic morphogenesis

(A) Representative images of P21 Ang1$^{flox/flox}$, NesCre:Ang1$^{+/flox}$, and NesCre:Ang1$^{flox/flox}$ stained with Calbindin (PC marker). Scale bar, 1 mm (top panels) and 100 µm (bottom panels).

(B) Bar graph showing ML thickness at P21 in all cerebella lobes (II–X).

(C) Bar graph showing PC number per 100 µm in lobes V and IX.

Data in (B) and (C) are shown as mean ± SEM from a minimum of n = 6 animals per genotype. Data are not significant if not indicated. One-way ANOVA for each lobe; *p < 0.05.

(D) Bar graph showing normalized bodyweight at P21 for the indicated mice. Data are represented as mean ± SEM from a minimum of n = 14 animals. One-way ANOVA; ****p < 0.0001.

(E) Representative image of traced PCs of $Ang1^{flox/flox}$, NesCre:$Ang1^{+/flox}$, and NesCre:$Ang1^{flox/flox}$ mice at P56.

(F and G) Quantitation of the number of branches and total dendritic length at P56. Data are represented as mean ± SEM from a minimum of n = 11 neurons from a minimum of 3 independent animals. One-way ANOVA; *p < 0.05; **p < 0.01; ****p < 0.0001.

(H) Representative PC traces of PCs from organotypic cerebellar slices from P6 pups stimulated with or without 100 ng/mL rAng1 over the course of 3 DIV.

(I and J) Quantitation of the number of branches and total dendritic length of PCs from cerebellar slices. Data are represented as mean ± SEM from a minimum of n = 24 neurons from a minimum of 4 independent experiments. Unpaired Student's t test; *p < 0.05.

(K) Representative images of P21 $Ang2^{+/-}$ and $Ang2^{-/-}$ cerebella sections stained with Calbindin. Scale bar, 1 mm and 100 μm in higher magnification.

(L) Bar graph showing ML thickness at P21 in all cerebella lobes (II–X).

(M) Bar graph showing PC number per 100 μm in lobes V and IX.

Data in (L) and (M) are represented as mean ± SEM from a minimum of n = 3 animals. Data are not significant if not indicated. One-way ANOVA for each lobe.

(N) Bar graph showing normalized bodyweight at P21 for the indicated mice. Data are represented as mean ± SEM from a minimum of n = 8 animals. Data are not significant if not indicated. One-way ANOVA; *p < 0.05.

(O) Representative traced PCs of WT, $Ang2^{+/-}$, and $Ang2^{-/-}$ mice at P56.

(P and Q) Quantitation of the number of branches and total dendritic length of WT, $Ang2^{+/-}$, and $Ang2^{-/-}$ mice at P56.

Data are represented as mean ± SEM from a minimum of n = 11 neurons from a minimum of 3 independent animals. One-way ANOVA; *p < 0.05; **p < 0.01; ***p < 0.001. Scale bars in (E), (H), and (O), 50 μm. See also Figures S5 and S6.

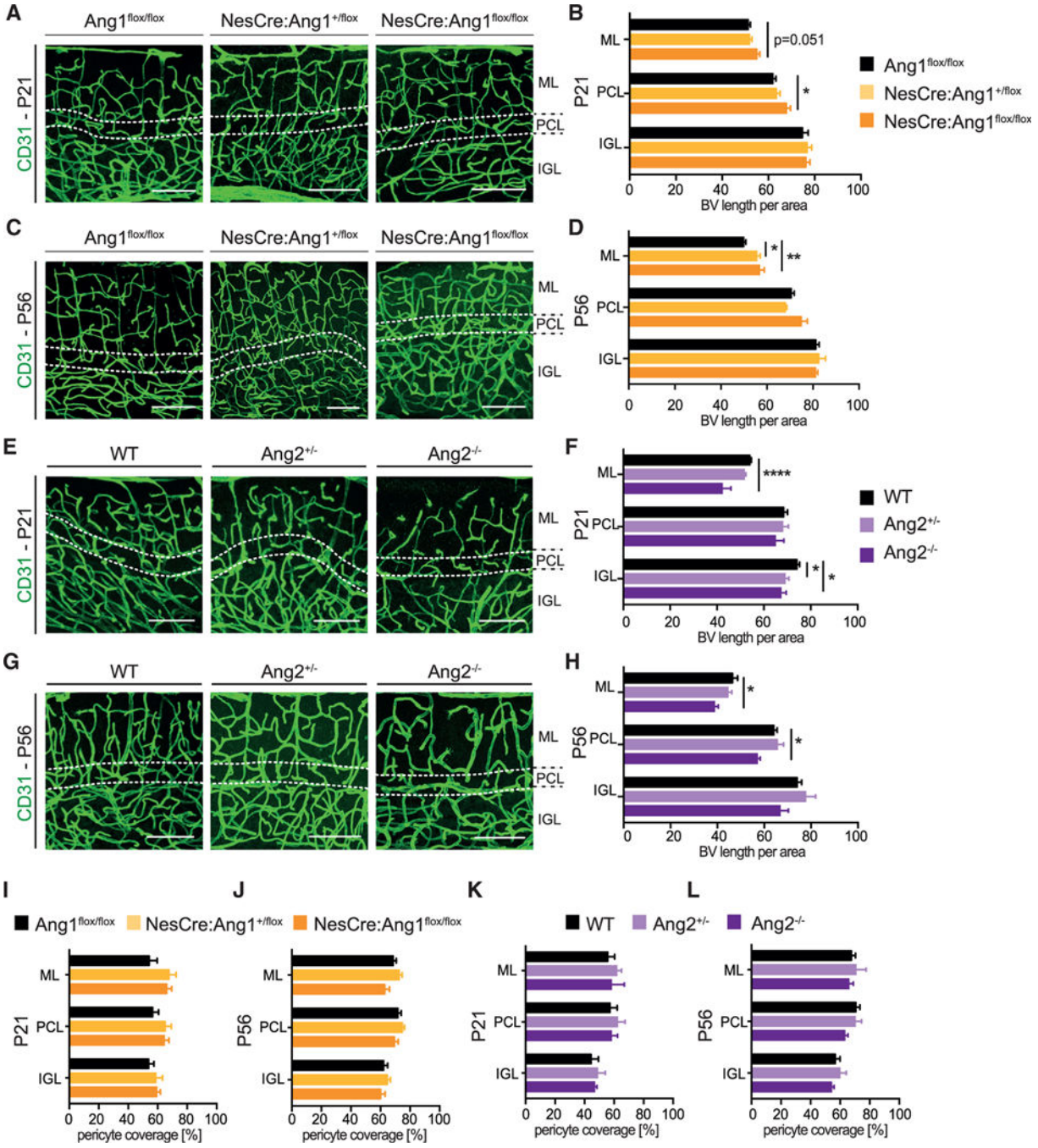

Figure 4. NesCre:Ang1$^{flox/flox}$ and Ang2$^{-/-}$ mice show mild vascular morphological defects in the cerebellum

(A and C) Representative images of blood vessels (stained with the EC marker CD31) in the cerebellum from P21 and P56 from Ang1$^{flox/flox}$, NesCre:Ang1$^{+/flox}$ and NesCre:Ang1$^{flox/flox}$ animals.

(B and D) Quantification of blood vessel length per area, for the different cerebellar layers. Data are represented as mean ± SEM from a minimum of n = 3 animals. Data are not significant if not indicated. One-way ANOVA; *p < 0.05; **p < 0.01.

(E and G) Representative images of blood vessels (stained with the EC marker CD31) in the cerebellum from P21 and P56 from WT, $Ang2^{+/-}$, and $Ang2^{-/-}$ mice.
(F and H) Quantification of blood vessel length per area for the different cerebellar layers. Data are represented as mean ± SEM from a minimum of n = 3 animals. Data are not significant if not indicated. One-way ANOVA; *p < 0.05; ****p < 0.001. Scale bar in (A), (C), (E), and (G): 100 μm.
(I–L) Pericyte coverage of blood vessels in the cerebellum was quantified in the different cerebellar layers at P21 (I and K) and P56 (J and L) for the indicated mice. Data are represented as mean ± SEM from a minimum of n = 3 animals. Data are not significant if not indicated. One-way ANOVA.

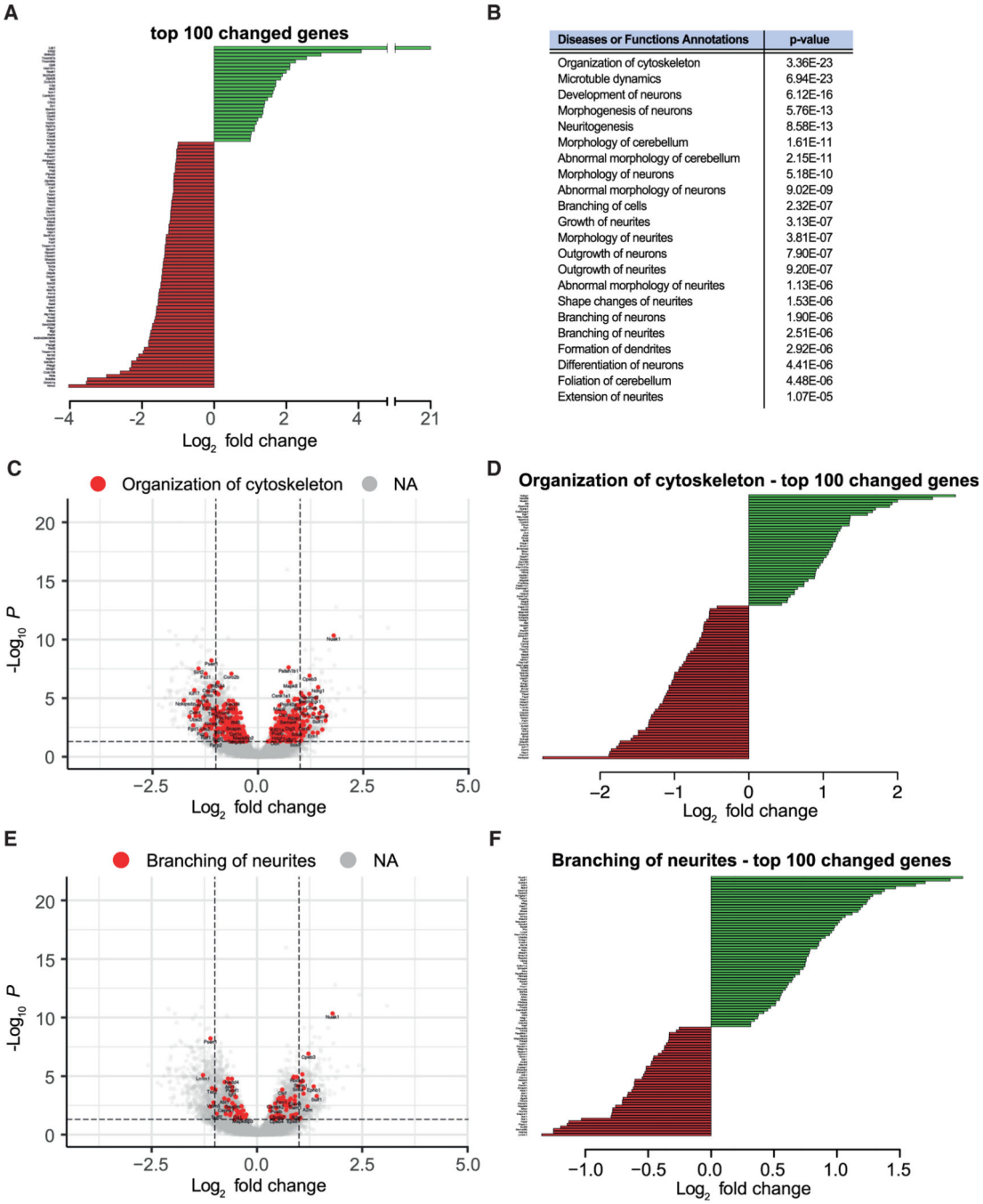

Diseases or Functions Annotations	p-value
Organization of cytoskeleton	3.36E-23
Microtuble dynamics	6.94E-23
Development of neurons	6.12E-16
Morphogenesis of neurons	5.76E-13
Neuritogenesis	8.58E-13
Morphology of cerebellum	1.61E-11
Abnormal morphology of cerebellum	2.15E-11
Morphology of neurons	5.18E-10
Abnormal morphology of neurons	9.02E-09
Branching of cells	2.32E-07
Growth of neurites	3.13E-07
Morphology of neurites	3.81E-07
Outgrowth of neurons	7.90E-07
Outgrowth of neurites	9.20E-07
Abnormal morphology of neurites	1.13E-06
Shape changes of neurites	1.53E-06
Branching of neurons	1.90E-06
Branching of neurites	2.51E-06
Formation of dendrites	2.92E-06
Differentiation of neurons	4.41E-06
Foliation of cerebellum	4.48E-06
Extension of neurites	1.07E-05

Figure 5. PC-specific loss of Tie2 leads to alterations in the expression of genes involved in neuronal wiring

(A) The PC translatome was sequenced form Pcp2Cre:Rpl22$^{HA/HA}$ and Pcp2Cre:Tie2$^{flox/flox}$:Rpl22$^{HA/HA}$ animals at P56. The top 100 gene changes (by adjusted p value) are shown ranked by unmodified log2 fold change.

(B) Shortened list of affected pathways analyzed with ingenuity pathway analysis (IPA).

(C–F) Among annotations, “organization of cytoskeleton” (C and D) and “branching of neurites” (E and F) are shown. Total gene changes (IfcShrink fold change) are visualized by

volcano plot in (C) and (E). The top 100 up- and downregulated genes of the annotations are shown ranked by unmodified log2 fold change in (D) and (F).
See also Figure S7.

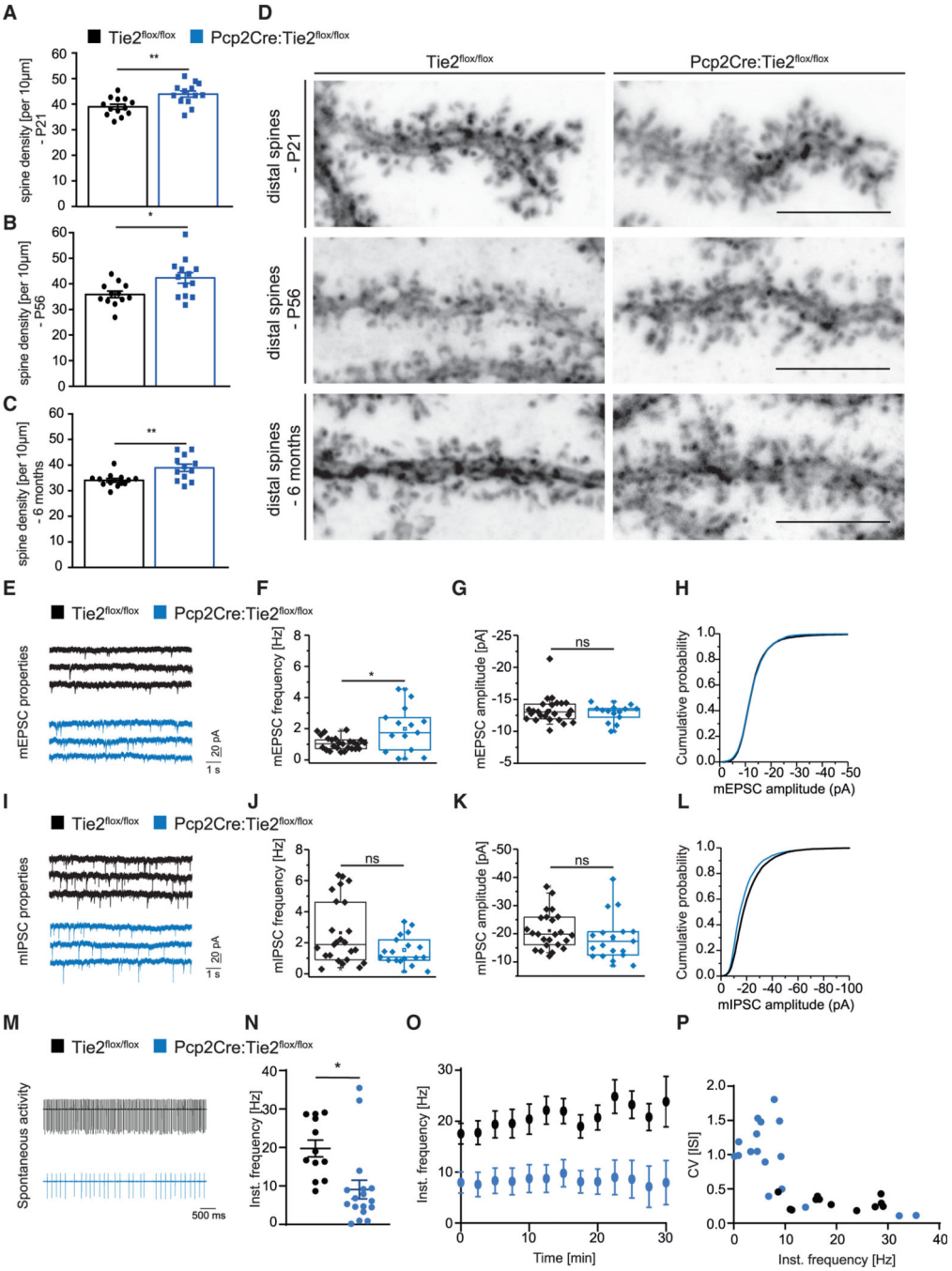

Figure 6. Loss of Tie2 expression in postnatal PCs results in alterations of cerebellum network functionality

(A–D) Distal dendritic spines were counted in AAV8-transduce PCs of Tie2$^{flox/flox}$ and Pcp2Cre:Tie2$^{flox/flox}$ animals at P21 (A and D), P56 (B and D), and 6 months (C and D). Data are represented as mean ± SEM from a minimum of n = 10 neurons from a minimum of three independent animals. Unpaired Student's t test; *p < 0.05; **p < 0.01. Representative pictures are shown in (D). Scale bar: 5 µm.

(E–L) PCs of Tie2$^{lox/lox}$ and Pcp2Cre:Tie2$^{flox/flox}$ animals were patched at 8–11 weeks of age and mEPSCs (E–H) and mIPSCs (I–L) were recorded. Example traces are shown in (E)

and (I). Event frequency (F and J), amplitude (G and K), and cumulative probability (H and L) are shown. Data are represented as boxplot from a minimum of n = 14 neurons from a minimum of 4 independent animals.

(M–P) PCs of $Tie2^{lox/lox}$ and Pcp2Cre:$Tie2^{flox/flox}$ animals were patched at 8–11 weeks of age and spontaneous tonic firing was recorded. Example traces are shown in (M). Instantaneous frequency (N–P) was analyzed. Data are represented as mean ± SEM from a minimum of n = 12 neurons from a minimum of 3 independent animals. Unpaired Student's t test; *$p < 0.05$; ns, not significant. See also Figure S4.

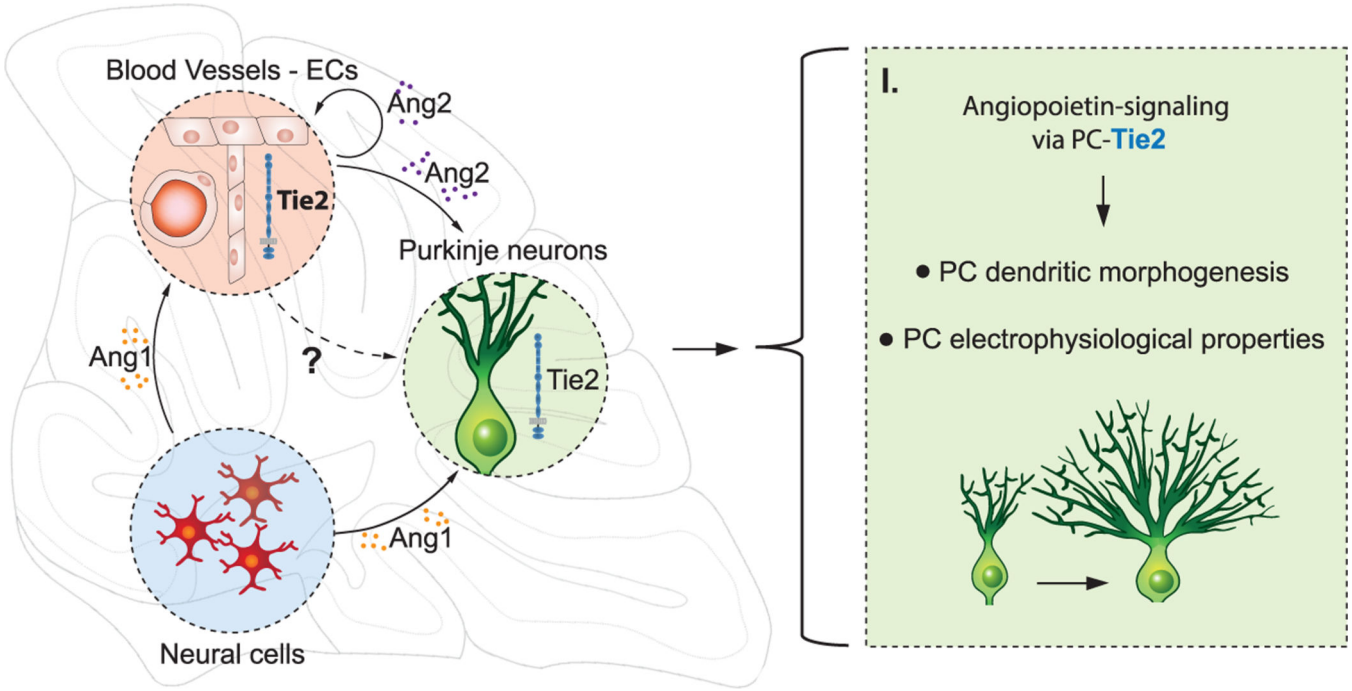

Figure 7. Proposed model of Tie2 cell-autonomous effect in PCs

During development of the mouse cerebellum, Ang1 expressed by neural cells and Ang2 expressed by ECs signal to Tie2, expressed in PCs to modulate dendritic morphogenesis and electrophysiological properties. Angiopoietin ligands expressed during the postnatal development also contribute to the proper formation of the vasculature in the cerebellum, via Tie2 signaling in ECs.

KEY RESOURCES TABLE

REAGENT or RESOURCE	SOURCE	IDENTIFIER
Antibodies		
Rabbit polyclonal anti-Ang1	Abcam	ab8451
anti-chicken-Alexa488	Molecular Probes	A11039
anti-goat-Alexa488	Jackson ImmunoResearch	705–545-033
anti-goat-Alexa568	Molecular Probes	A11057
anti-mouse-Alexa488	Jackson ImmunoResearch	115–545-146
anti-mouse-Alexa568	Invitrogen	A11031
anti-rabbit-Alexa488	Invitrogen	A11008
anti-rabbit-Alexa488	Invitrogen	711–545-152
anti-rabbit-Alexa568	Jackson ImmunoResearch	A10042
anti-rat-Alexa594	Molecular Probes	A21209
Mouse monoclonal anti-CALBINDIN-D-28K(clone CB-955)	Sigma-Aldrich	C9848
Rat monoclonal anti-CD13	Bio-Rad	MCA2183GA
Goat polyclonal anti-CD31	R&D	AF3628
DAPI	Invitrogen	D1306
Goat polyclonal anti-GFAP	Abcam	ab53554
Chicken polyclonal anti-GFP	Aves	GFP-1020
IsolectinB-Alex568	Invitrogen	I21412
Mouse monoclonal anti-OLIG2	Millipore	MABN50
TO-PRO-3	Invitrogen	T3605
Chemicals, peptides, and recombinant proteins		
Agarose	Sigma-Aldrich	A9538
Ampicillin sodium salt	Sigma-Aldrich	A9518
Anti-HA-tag mAb-Magnetic Beads	MBL	M180–11
Bovine Serum Albumin (BSA)	Roth	8076.2
Calcium chloride dihydrate	AppliChem	A3587
cDNA synthesis SuperScript® Vilo	Invitrogen	11754–050
D(+)-Saccharose	Roth	4621.1
Deoxynucleotides (dNTPs)	NEB	N0447S
DEPC	Sigma-Aldrich	D5758
Dextran Sulfate Sodium (DSS)	MP Biomedicals	SKU 0216011050
DIG Blocking Reagent	Roche	11096176001
Digoxigenin (DIG) RNA labeling kit	Roche	11175025910
Dimethylsulfoxid (DMSO)	Gruesing	10282
DNA ladder 1 kb	Thermo Scientific	SM0311
DNA ladder 100 bp	NEB	N3231S
DNA loading dye (6×)	Thermo Scientific	P0611
DNA stain	Serva	39803.01

REAGENT or RESOURCE	SOURCE	IDENTIFIER
Antibodies		
DNase I, Rnase-free	Thermo Scientific	EN0521
DNaseI	Sigma-Aldrich	4716728001
EDTA	AppliChem	A3553
Ethanol	Sigma-Aldrich	32205
Fast Green FCF	Sigma-Aldrich	F7252
Fast SYBR Green Master Mix	Thermo Scientific	408995
Fluoromount-G	Linaris	0100–01
Formamid	Sigma-Aldrich	47670
Gelatine from porcin skin	Sigma-Aldrich	G1890
GenElute Plasmid Miniprepkit	Sigma-Aldrich	PLN70–1Kt
Hydrochloric acid solution, 1 M	Sigma-Aldrich	35328
Isofluran	Sigma-Aldrich	792632
Isopropanol	VWR	ACRO423830010
Ketamin (10%)	Bremer Pharma GmbH	27015.00.00
LB-Medium (BactoTMAgar)	BD	214010
LB-Medium (BactoTMTryptone)	BD	211705
LB-Medium (BactoTMYeast Extract)	BD	212750
Levamisol	Sigma-Aldrich	BP212
Lidocain	Aspen Pharma Trading Limited	PL 39699/0086
Magnesium chloride	AppliChem	A3618
Maleic acid	Sigma-Aldrich	M0375
mAng1 recombinant protein	R&D Systems	9936-AN
mAng2 recombinant protein	R&D Systems	7186-AN
Maxima Reverse Transcriptase	Thermo Scientific	EP0742
Methanol	Sigma-Aldrich	32213
Mowiol® 4–88	Sigma-Aldrich	81381
NBT/BCIP	Promega	S3771
NEB T4 DNA Ligase	NEB	M0202
NEG-50TM	Thermo Scientific	6502
Normal donkey serum	Dianova	017–000-121
Normal goat serum	Dianova	005–000-121
NucleoSpin® Gel and PCR Clean-Up	Nachery-Nagel	740609.25
PCR-CleanUp	Promega	A9281
Phosphate Buffer Saline	Sigma-Aldrich	D8537
Plasmid *Plus* MAXI kit	QIAGEN	12963
Potassium chloride	AppliChem	A3582
Potassium dihydrogenphosphate	AppliChem	A3620
Q5® HighFidelity DNA Polymerase	NEB	M0491
Sodium bicarbonate	Sigma-Aldrich	31437
Sodium chloride	Sigma-Aldrich	31434

REAGENT or RESOURCE	SOURCE	IDENTIFIER
Antibodies		
Sodium dodecyl sulfate (SDS)	Roth	CN30.3
Sodium hydroxyde	Sigma-Aldrich	30620
Sodium phosphate dibasic dihydrate	Sigma-Aldrich	4272
Sodium phosphate monobasic monohydrate	Sigma-Aldrich	71504
Tissue-Tek® O.C.T. Compound	Genprice	4583
Tneasy® Mini kit	QIAGEN	74104
Torula RNA	Merck	10109223001
tris(hydroxymethyl)aminoethane (TRIS)	Roth	4855.2
Triton X-100	Merck	108603
TRIzol Reagent	Thermo Scientific	15596026
Trypsine-EDTA	Sigma-Aldrich	T3924
Tween®20	Roth	9127.1
Wizard®SV Gel and PCR CleanUp System	Promega	A9281
Xylavet (20 mg/ml)	CP-Pharma Handelsges. mbH	401510.00.00
Deposited data		
RNA-seq data	this study	GSE178659
Experimental models: Organisms/strains		
$Ang1^{flox/flox}$	(Jeansson et al., 2011)	N/A
$Ang2^{-/-}$	(Hu et al., 2014)	N/A
NesCre	(Tronche et al., 1999)	N/A
Rosa26:mTomato-mGFP	(Muzumdar et al., 2007)	N/A
	Jackson Laboratories	
	JAX stock #007676	
Pcp2Cre	(Barski et al., 2000)	N/A
$Rpl22^{HA/HA}$	(Sanz et al., 2009)	N/A
	Jackson Laboratories	
	JAX stock #011029	
$Tie2^{flox/flox}$	(Savant et al., 2015)	N/A
Tie2-GFP	(De Palma et al., 2005)	N/A
Oligonucleotides		
See Table S3		N/A
Software and algorithms		
DEseq2	(Love et al., 2014)	https://bioconductor.org/packages/release/bioc/html/DESeq2.html

REAGENT or RESOURCE	SOURCE	IDENTIFIER
Antibodies		
FastQC	Freeware (Andrews, 2010)	https://www.bioinformatics.babraham.ac.uk/projects/fastqc/
Fiji - ImageJ	Freeware (Schindelin et al., 2012)	https://imagej.net/software/fiji
GraphPad Prism 6/7	GraphPad Software	https://www.graphpad.com
HTSeq-count	(Anders et al., 2015)	https://htseq.readthedocs.io/en/release_0.11.1/overview.html
IMARIS 8.4.2	Bitplane AG	https://imaris.oxinst.com/
IPA	QIAGEN Inc. (Krämer et al., 2014)	https://digitalinsights.qiagen.com/products
Microsoft Office	Microsoft	https://office.live.com/start/Excel.aspx
R	Freeware (R Team, 2020)	https://cran.r-project.org/
samtools	(Li et al., 2009)	http://www.htslib.org/
STAR	(Dobin et al., 2013)	https://github.com/alexdobin/STAR